**Optimal Design of Anti-Reflection Coatings for Solar Cells Using the Method of the Approximate Inverse and its Extension**

# Dissertation

zur Erlangung des Grades des

**Doktors der Naturwissenschaften**

der Naturwissenschaftlich-Technischen Fakultäten
der Universität des Saarlandes

vorgelegt von

**Mohammad Alakel Abazid, M.Sc.**

Saarbrücken, 2014

| | |
|---|---|
| Tag des Kolloquiums: | 02. Juli 2014 |
| Dekan: | Univ.-Prof. Dr. Markus Bläser |
| Vorsitzender: | Univ.-Prof. Dr. Jörg Eschmeier |
| Berichterstatter | Univ.-Prof. Dr. Dr. h.c. mult. Alfred K. Louis |
| | Univ.-Prof. Dr. Sergej Rjasanow |
| Akademischer Mitarbeiter: | Dr. Aref. Lakhal |

# Kurze Zusammenfassung

In dieser Arbeit wird das inverse Streuproblem für Wellen, die bei der optischen Schicht auf Solarzellen auftritt, untersucht. Das Ziel ist es, den ortsabhängigen Brechungsindex in einer solchen inhomogenen Schicht zu optimieren um eine Verbesserung der Leistungsfähigkeit der Solarzellen zu erreichen. Das zugehörige Berechnungsmodell besteht aus einem Randwertproblem für die eindimensionale Helmholtz-Gleichung, aus der wir eine Integralgleichung ableiten. Das inverse Problem ist nicht linear und schlecht gestellt. Als erste Möglichkeit wird die Born-Approximation verwendet, um das mathematische Modell zu linearisieren. Zur Regularisierung des formulierten inversen Problems benutzen wir die Methode der Approximativen Inversen. Zum Vergleich führen wir ebenfalls numerische Tests mit Hilfe der Tikhonov-Phillips Methode durch. Als alternative Herangehensweise lösen wir das nicht-lineare Problem unter Verwendung des Approximativen Inversen für quadratische Probleme. Numerische Ergebnisse werden vorgestellt, um die Effizienz der verschiedenen Methoden zu vergleichen.

# Abstract

We consider the inverse scattering problem arising in an optical coating deposited onto photovoltaic solar cells. Our objective is to optimize the space-dependent refractive index in this inhomogeneous cover to enhance the efficiency of the solar cells. The relevant model yields a boundary value problem for the one-dimensional Helmholtz equation, from which we derive an equivalent integral equation formulation. The resulting inverse problem is nonlinear and ill-posed. Firstly, we use the Born approximation to linearize the mathematical model. For regularizing, we apply the method of the Approximate Inverse. For the purpose of comparison, we also make numerical tests using Tikhonov-Phillips as a regularization method. Secondly, we treat the nonlinear problem using the method of the Approximate Inverse for the quadratic problem. Numerical results are presented to compare the efficiency of the methods.

# Contents

# List of Symbols

| | |
|---|---|
| ARC | Anti-Reflection Coating |
| BVP | Boundary value problem |
| | |
| $\lambda$ | Wave length |
| $\omega$ | Angular frequency |
| $c$ | Speed of light |
| $\kappa$ | Free space wave number |
| $k$ | Integral kernel |
| $k^2$ | Second iterated integral kernel |
| $K$ | Integral operator |
| $L$ | Differential operator |
| $\beta$ | Nondimensionnalised wave number |
| $d$ | Thickness of the ARC |
| $\mu_0$ | Magnetic permeability in free space |
| $\varepsilon_0$ | Electric permittivity in free space |
| $n_0$ | Refractive index of vacuum |
| $n_s$ | Refractive index of glass |
| $n_{si}$ | Refractive index of silicon |
| $n(x)$ | Refractive index of the ARC |
| $u$ | Magnitude of the electromagnetic field |
| $u^0$ | incident field |
| $u^s$ | scattered field |
| $\nabla$ | Gradient |
| $\nabla\cdot$ | Divergence |
| $\nabla\times$ | Curl |
| $\Delta$ | Laplace operator |

| | |
|---|---|
| $g$ | Green's function |
| $G$ | Gram matrix |
| $A$ | Linear operator |
| $\mathcal{A}$ | Nonlinear operator |
| $A_1$ | Linearized operator of the model |
| $A_2$ | Quadratic operator of the model |
| $A^*$ | Adjoint operator of $A$ |
| $A^\dagger$ | Generalized inverse of $A$ |
| $\mathcal{D}(A)$ | Domain of operator $A$ |
| $\mathcal{N}(A)$ | Null space of operator $A$ |
| $\mathcal{R}(A)$ | Range of operator $A$ |
| | |
| $\mathcal{R}(\beta)$ | Reflection coefficient |
| $\mathcal{T}(\beta)$ | Transmission coefficient |
| | |
| $C(\Omega)$ | Space of continuous functions on an open set $\Omega \in \mathbb{R}^m, m \in \mathbb{N}$ |
| $C^m(\Omega)$ | Space of $m$-times continuously differentiable functions on $\Omega$ |
| $L_2(\Omega)$ | Space of squared integriable functions on $\Omega$ |
| $\langle ., . \rangle$ | Scalar product in $L_2(\Omega)$ |
| | |
| $\gamma$ | Regularization parameter |
| $\delta^\gamma$ | Mollifier |
| $\delta_{\text{lin}}$ | Relative error in the linear approximation |
| $\delta_{\text{quad}}$ | Relative error in the quadratic approximation |
| $\psi^\gamma$ | Reconstruction kernel |
| $\mathcal{I}$ | Identity operator |
| $M^T$ | Transpose matrix of M |
| AI | The method of the Approximate Inverse |
| TP | The method of Tikhonov-Phillips |

# Introduction

Depositing **Anti-Reflection Coatings (ARCs)** is essential for producing solar cells. More than 35% of the incident sunlight can be lost by normal installation without using ARCs. To enhance the efficiency of photovoltaics, an ARC is laid on the surface of the cell, [10,11]. Depositing these thin films with appropriate refractive index onto the solar cells traps the sun light which should remain propagating between two media with two different refractive indices, see Figure (1). As a result, one saves the sunlight inside by minimizing or eliminating the light reflection.

Besides photovoltaics, ARCs are widely used to ensure the decreasing of the light reflection in various application areas including displays, telescopes, microscopes, ophthalmics, and camera lenses.

A different approach is the diffraction gratings [9,17,20], where a periodic structure of the surface is to be determined.

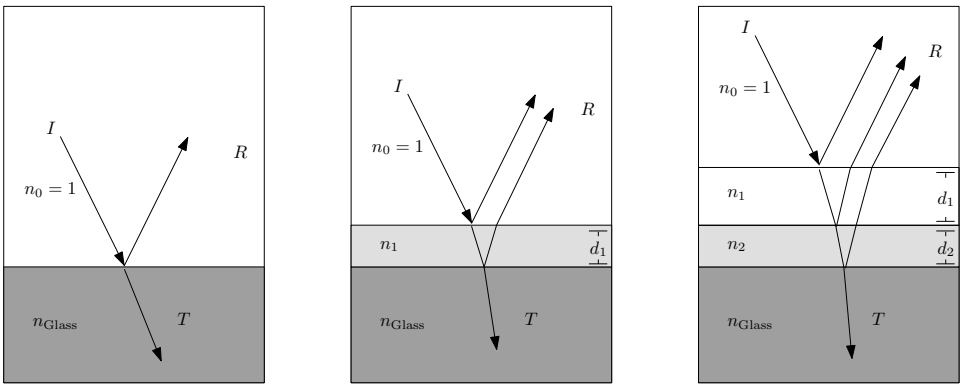


**Figure 1: Anti-Reflection Coatings (ARCs)** (1) Old setting of solar cell without ARC. (2) Single-layer ARC with thickness $d_1$ in contact with a glass substarate. (3) Double-layer ARC in contact with a glass substarate.

ARCs, in their simplest settings, are designed for one-layer with a single wavelength $\lambda$ at normal incidence. An approximately-complete cancellation of the reflection occurs when the refractive index is equal to the geometric mean of the refractive indices of the ambient upper and lower media, namely

$n_{\text{ARC}} = n = \sqrt{n_0 n_s}$ and $\lambda = 4dn$. The parameters $n, n_0$, and $n_{\text{Glass}} = n_s$ stand for the refractive indices of the coating, free space, and the glass, respectively. The parameter $d$ is the thickness of the coating. This cancellation of the reflection happens when the coating has the refractive index $n = 1.23$. However, this possibility assumes that the ARC has one constant refractive index. Moreover it works only for one wavelength. In contrast to uni-layer films, multi-layer coatings reduce the reflections throughout a wide range of the wavelengths, [6, 16, 54]. In this multi-layer setting, the coating is a stack of homogeneous layers with different constant refractive indices. Another additional setting for the ARC is to use a coating with space-dependent refractive index. A graded-index ARCs with varying index of refraction assures more absorbed energy and achieves best performance [41, 49]. Therefore, we consider in our research a coating, which is inhomogeneous *i.e.*, its refractive index $n$ varies in the space $x$, [2, 3, 31]. Both cases of the single-layer with a constant refractive index or the multi-layer with a piece-wise constant refractive index, are special cases of this setting.

The design of ARC is usually achieved in a direct way. In this direct design method, a prototype with specified optical properties of the coating is considered, and the generated electromagnetic field is investigated. The constitutive properties are calibrated until the desired effect is realized. However, the practical improvement of the coating design requires dealing with internal quantities, namely the refractive index. Dealing with such internal quantity requires solving the inverse problem of the related mathematical model. Therefore, solving the inverse problem is the main task in our research. The objective in the inverse problem is to determine the refractive index of the ARC from the given values of the electromagnetic field at the surface. These given values represent the reflection coefficients, which are the input data for solving the inverse problem.

The nature of the problem treated in this work is closely related to the concept of cloaking [4]. The objective in such an application is to make a target invisible with respect to probing by electromagnetic waves. Cloaking happens when a body of dielectric material is coated by a plasmonic structure of "negative" dielectric constant. The approach in [5] proposes a new cancellation technique in order to achieve enhanced near invisibility.

For modeling the light propagation through a stratified isotropic non-magnetic medium the corresponding time-harmonic Maxwell's equations are

$$\begin{cases} \nabla \times \mathbf{E} - i\omega\mu_0 \mathbf{H} &= 0, \\ \nabla \times \mathbf{H} + i\omega\varepsilon(x)\mathbf{E} &= 0, \end{cases} \tag{0.1}$$

where $\mathbf{E}$ and $\mathbf{H}$ are the electric and magnetic vector fields respectively. The parameter $\omega$ denotes the angular frequency, while $\mu_0$ is the magnetic permeability of the free space. The function $\varepsilon(x)$ is the dielectric permittivity of the

coating. In Chapter 1, we discuss in detail the Maxwell's equations, which describe the propagation of an electromagnetic wave. From these equations, we derive in Chapter 2 the related mathematical model. Since the ARC is assumed to be in a bounded volume, the resulting model is prescribed as a boundary value problem (BVP) for the one-dimensional Helmholtz equation:

$$(\text{BVP}) \begin{cases} u''(x) + \beta^2 n^2(x) u(x) = & 0, \ x \in (0,1), \\ u'(0) + i n_0 \beta u(0) = & 2 i n_0 \beta, \\ u'(1) - i n_s \beta u(1) = & 0. \end{cases} \tag{0.2}$$

The equation $n^2(x) = 1 + f(x)$ relates refractive index $n(x)$ to the contrast function $f(x)$ of the ARC. The variable $u$ denotes the magnitude of the field, the second derivative of the field is $u''$. The parameter $\beta = \kappa d$ denotes the nondimensionalised wave number where $\kappa = 2\pi/\lambda$ is the free space wave number, and $\lambda$ is the wave length.

In Chapter 2, we transform the model (0.2) into an equivalent integral equation formulation. As a result, we obtain the Fredholm integral equation of the second kind

$$u(x) + \beta^2 \int_0^1 k_\beta(x,y) f(y) u(y) dy = u^0(x), \ x \in (0,1), \tag{0.3}$$

where $u^0(x)$ is the incident field and $k_\beta(x,y)$ is the integral kernel which satisfies the boundary conditions in the BVP (0.2). In the scattering theory, equation (0.3) is known as Lippmann-Schwinger integral equation [13].

To generate the data of the inverse problem, we solve the direct problem. Based on a Nyström quadrature method, we develop a direct solver using Matlab. Depending on a given incident field impinging upon the ARC, the direct solver determines the total field for a given contrast function. This, in turn, produces the reflection coefficients which are the differences between the values of the incident and the total fields on the surface. The direct solver program offers a crucial advantage when dealing with space-dependent contrast function. This is due to lacking an explicit analytic formula for the related total field. For more details, we refer to the discussion in Chapter 4.

The general existing methods to solve the inverse scattering problem depend on two approaches. Whether using nonlinear techniques by applying iterative algorithms or using linearized inversion schemes. The nonlinear methods reconstruct the unknowns of the problem iteratively from *a priori* guess. These methods solve usually a sequence of forward problems using techniques such as the finite difference schemes, as done in [41], where the regularization method of Tikhonov-Phillips is used to solve the relevant nonlinear problem in the sense of least squares. As opposed to nonlinear techniques, the linearized inversion schemes are based on approximations of Born or Rytov type, which are valid for media with low contrasts. As an application of this Approximation, consult [2, 25].

To solve our inverse scattering problem, we face two main difficulties. The first is the nonlinearity; the field depends on the contrast function of the object in a nonlinear manner. The second is the ill-posedness of the problem, since small errors on the data, no matter how small they are, result with large errors on the solution, which is typical for inverse problems.

We use Born approximation for linearizing the mathematical model of our problem. Consult [32, 53]. In this approximation, we assume that the scattered field is very small compared to the incident field. Having the scattered field sufficiently small, so that it can be neglected, allows for extracting a linearized form of the problem as we do in Chapter3. The Born approximation is practical and feasible under some important limitations on the contrast function, and on the relevant range of the wave numbers.

The ill-posedness of the inverse problem is twofold. This is due to non-uniqueness and ill-conditioning. The application of a regularization method is then required to stabilize the solution [36, 37], and [38]. We refer to [42], and [45] for a general analytical study on the regularization of ill-posed problems. A short related discussion can be found in Chapter 3.

The method of the Approximate Inverse (AI) is a stable and flexible regularization scheme. This method, introduced by Louis and Maass [48], and analyzed by Louis [43], is used as a main regularization method in this work. It is an efficient method for solving linear problems [45] and nonlinear problems [43,44]. It has been extended for image reconstruction [46], feature extraction [47], and for solving inverse problems on Banach-spaces [35, 58].

To briefly describe the AI method for solving the linearized problem, let $A : X \longrightarrow Y$ denote a linear non-degenerate compact operator between the Hilbert spaces $X \subset L_2(\Omega)$ and $Y \subset L_2(\Gamma)$, on some measurable sets $\Omega$ and $\Gamma$, endowed with the scalar product $\langle ., . \rangle$. This method finds a stable solution $f$ to the equation $Af = g$ by computing the approximation $f_\gamma(x) = \langle f, \delta_x^\gamma \rangle_X$. The mollifier $\delta_x^\gamma$ is an approximation of the Delta distribution for the reconstruction point $x$. To find this mollifier, we solve the following auxiliary equation

$$A^* \psi_x^\gamma = \delta_x^\gamma, \tag{0.4}$$

where $A^*$ is the adjoint operator of $A$ and $\psi_x^\gamma$ is the reconstruction kernel. Thus, it holds

$$f_\gamma(x) = \langle f, \delta_x^\gamma \rangle_X = \langle f, A^* \psi_x^\gamma \rangle_X = \langle Af, \psi_x^\gamma \rangle_Y = \langle g, \psi_x^\gamma \rangle_Y =: S_\gamma g(x). \tag{0.5}$$

For solving the nonlinear problem, Louis [43] extended the previously mentioned method for some nonlinear problems. In Chapter 3, we apply this extension to approximate the nonlinear problem of our model (0.3). Moreover, we introduce the efficient concept of the adaptive modeling, where we use a threshold to decide locally where to apply a higher (quadratic) order

of approximation. We take here advantage of the method of the Approximate Inverse which is a local method. We use a criterion which evaluates the quality of the linear reconstruction in every part of the function $f$.

Let us briefly outline the contents of this thesis. In Chapter 1, we introduce Maxwell equations which will be needed for deriving our mathematical model. Furthermore, the derivation is completely developed as a boundary value problem (BVP) in Chapter 2. The resulting BVP is transformed into an equivalent integral equation of Lippmann-Schwinger type. In Chapter 3, the inverse nonlinear problem of the model (0.3) is formulated and then linearized using the first iteration of the Born approximations. The second iteration of the Born approximations yields the quadratic approximation of the nonlinear problem which is discussed in the same chapter. Moreover, the application of the method of Approximate Inverse to solve the linearized problem as well as to quadratically approximate the nonlinear problem is also treated in Chapter 3. Chapter 4 is dedicated to the presentation and discussion of the numerical simulations. In the conclusion, we summarize the features characterizing our method. Finally, we give an outlook about some interesting issues for a future research. In Appendix A, we present some relevant details about solar cells and Anti-Reflection Coatings including the transmission and reflection coefficients $T$ and $R$ respectively.

# Acknowledgements

At the very beginning, I would like to express my deep gratitude to my supervisor Univ.-Prof. Dr. Dr. h.c. mult. Alfred K. Louis; not only did he supervise my thesis with a professional expertise, but he also offered me the great opportunity of joining his team of qualified researchers. While working in his group I gained an invaluable research experience in the exciting field of applied mathematics. For his substantial support, I am so grateful.

Secondly, I would like to deeply thank my advisor Dr. Aref Lakhal for the encouragement, invaluable advice and discussions, and the scientific support he offered me during this work. His constant support was central to the successful achievement of the milestones of my Ph.D. studies. I am glad I had my research experience under his insightful guidance.

I would like to acknowledge all the former and current colleagues for assuring a nice and cooperative atmosphere during the period of my Ph.D. studies. Special thank to Dr. Martin Riplinger and Dr. Gael Rigaud for the many valuable and technical remarks.

I am also thankful to all the people, relatives, and friends who helped me to overcome the many burdens and difficulties I encountered during the time of my Ph.D. studies.

Many thanks are due to all the foundations and universities that granted me scholarships, enabling me to successfully pursue my scientific ambitions.

I would like to express my deepest gratitude to my parents; to my mother who always offered me her best so heartily and so willingly, and to my father, whom to his soul I dedicate this thesis. It is so vivid my memory of him, taking care of me and motivating me till he left this life a few months ago.

Deeply from my heart, I thank my dear wife for her love, patience, steady support, motivation, and assistance. I express my gratitude to her and my best wishes to my children.

# Chapter 1

# Electromagnetic Scattering

The design of Anti-Reflection Coatings requires a good understanding of the behavior of electromagnetic waves in inhomogeneous media. Therefore, we shed the light in this chapter on the Maxwell's equations which describe the propagation of an electromagnetic wave. We refer basically to [13], [14], [18], [39], and [52] for the contents of this chapter.

## 1.1 The Maxwell equations

We start this section by introducing the equations of Maxwell which model the propagation of an electromagnetic wave in inhomogeneous media

$$\nabla \times \mathcal{E} = \mathcal{M} - \frac{\partial \mathcal{B}}{\partial t} \tag{1.1}$$

$$\nabla \times \mathcal{H} = \mathcal{J}_c + \mathcal{J}_e + \frac{\partial \mathcal{D}}{\partial t}, \tag{1.2}$$

where $\mathcal{E} = \mathcal{E}(x,t) \in \mathbb{C}^3$ and $\mathcal{H} = \mathcal{H}(x,t) \in \mathbb{C}^3$ are the complex-valued three-dimensional electric and magnetic vector fields in a space position $x = (x_1, x_2, x_3) \in \mathbb{R}^3$ at time $t \in \mathbb{R}$.

$\mathcal{D}$ is the electric flux density, $\mathcal{B}$ is the magnetic flux density, $\mathcal{J}_c$ is the conduction current density, $\mathcal{J}_e$ is the extraneous electric current source density, and $\mathcal{M}$ is the magnetic current source density.

The differential operators are denoted using the nabla operator $\nabla = (\partial_x, \partial_y, \partial_z)^T$ as $\nabla, \nabla\cdot$, and $\nabla\times$ indicate respectively the gradient, divergence, and the curl.

The constitutive equations relate the electric and magnetic flux densities $\mathcal{B}$ and $\mathcal{D}$ to the magnetic and electric intensities $\mathcal{H}$ and $\mathcal{E}$, respectively. Here we consider a *linear isotropic* medium:

$$\mathcal{B} = \mu\mathcal{H}$$
$$\mathcal{D} = \varepsilon\mathcal{E},$$

where $\mu$ is the *magnetic permeability* and $\varepsilon$ is the *electric permittivity*.

In the general case of *anisotropic medium*, $\mu$ and $\varepsilon$ are symmetric two-dimensional tensors specified to vectors formed with the corresponding eigenvalues. The medium is called *isotropic* if all the eigenvalues of each tensor are equal, here we may refer to [8].

Thus, the underlying medium is assumed to be isotropic and also *inhomogeneous*, this means its permeability and permittivity are real valued functions depending on the position $x$, $\mu = \mu(x)$ and $\varepsilon = \varepsilon(x)$. In the case of free space, the latter functions have constant values as $\mu = \mu_0$ and $\varepsilon = \varepsilon_0$.

The conduction current density $\mathcal{J}_c$ is determined by the electric field intensity $\mathcal{E}$ through *Ohm's law*

$$\mathcal{J}_c = \sigma_e \mathcal{E},$$

where $\sigma = \sigma_e(x)$ is the electric conductivity of the medium ranging between 0 and $\infty$ for a non-conducting and a perfect-conducting medium respectively.

The magnetic current source density $\mathcal{M}$ is related to the magnetic field intensity $\mathcal{H}$ through the following equation

$$\mathcal{M} = -\mathcal{J}_m + \sigma_m \mathcal{H},$$

where $\mathcal{J}_m = \mathcal{J}_m(x,t)$ is the complex-valued vector field which stands for the extraneous magnetic current density and $\sigma_m = \sigma_m(x)$ is the magnetic conductivity as a real-valued function.

Any electromagnetic field quantity is assumed to be time-harmonic *i.e.* it is periodic in time and can be written in terms of the real part operator as a product of spatial function and a periodic temporal function:

$$\mathcal{E}(x,t) = E(x,\omega)e^{-i\omega t},$$

$$\mathcal{H}(x,t) = H(x,\omega)e^{-i\omega t},$$

where $\omega > 0$ is the fixed angular frequency. Thus, the time-dependence of the electromagnetic fields can be suppressed using Fourier transform.

In addition to the electromagnetic fields, the current sources are assumed to be also time-harmonic:

$$\mathcal{J}_e(x,t) = J_e(x,\omega)e^{-i\omega t},$$

$$\mathcal{J}_m(x,t) = J_m(x,\omega)e^{-i\omega t}.$$

Under the time-harmonic assumption, the Maxwell's equations (1.1),(1.2) are reduced to the following time-independent system

$$\begin{aligned} \nabla \times \mathbf{E} - i\omega\tilde{\mu}\mathbf{H} &= -\mathbf{J}_m, \\ \nabla \times \mathbf{H} + i\omega\tilde{\varepsilon}\mathbf{E} &= \mathbf{J}_e, \end{aligned}$$

where the magnetic and the electric indices $\tilde{\mu}$ and $\tilde{\varepsilon}$ are complex valued functions defined as

$$\tilde{\mu}(x) := \mu(x) + i\frac{\sigma_m(x)}{\omega},\ x \in \mathbb{R}^3,$$

$$\tilde{\varepsilon}(x) := \varepsilon(x) + i\frac{\sigma_e(x)}{\omega},\ x \in \mathbb{R}^3,$$

with $\mu > 0, \quad \sigma_m \geq 0, \quad \varepsilon > 0, \quad \sigma_e \geq 0.$

The *refractive index* is defined by, (see [8])

$$n = \left(\varepsilon_0^{-1}\left(\varepsilon + i\frac{4\pi\sigma}{\omega}\right)\right)^{\frac{1}{2}}.$$

The *wave number* $\kappa$ is defined as

$$\kappa := \omega\sqrt{\varepsilon_0\mu_0}.$$

In order to introduce the direct electromagnetic scattering problem, we may assume that the extraneous current sources $\mathbf{J}_m$ and $\mathbf{J}_e$ are only generated in a bounded region and the medium is inhomogeneous in a bounded volume.

**Definition 1.1.** *Let $\Omega$ and $\Omega'$ be two bounded domains in $\mathbb{R}^3$ with smooth boundaries $\partial\Omega$ and $\partial\Omega'$, respectively. We assume that the closure sets $\overline{\Omega} := \partial\Omega \cup \Omega$ and $\overline{\Omega'} := \partial\Omega' \cup \Omega'$ do not intersect i.e. $\Omega \cap \Omega' = \emptyset$.*
*Furthermore we suppose*

1. *the complex valued functions $\tilde{\mu}$ and $\tilde{\varepsilon}$ are continuously differentiable on $\Omega$ and constant outside with $\mu(x) = \mu_0$ and $\varepsilon(x) = \varepsilon_0$ for $x \notin \Omega$.*

2. *the complex-valued vector fields $\mathbf{J}_m$ and $\mathbf{J}_e$ are continuous on $\Omega'$, and vanish outside i.e. $\mathbf{J}_m(x) = \mathbf{J}_e(x) = 0$ for $x \notin \Omega'$, and admit divergence fields $\nabla \cdot \mathbf{J}_m$ and $\nabla \cdot \mathbf{J}_e$, which are continuous on $\Omega'$.*

*The **direct electromagnetic scattering problem** is to determine the electromagnetic fields $\mathbf{E}$ and $\mathbf{H}$ by solving the time-harmonic Maxwell equations in $\mathbb{R}^3$, for given $\tilde{\mu}, \tilde{\varepsilon}, \mathbf{J}_m, \mathbf{J}_e$.*

The boundary conditions at infinity for Maxwell's equations are introduced in the following definition:

**Definition 1.2.** *Let the regular electromagnetic fields $\mathbf{E}, \mathbf{H}$, be solutions to the homogeneous Maxwell's equations*

$$\nabla \times \mathbf{E} - i\omega\mu_0 \quad \mathbf{H} = 0, \tag{1.3}$$

$$\nabla \times \mathbf{H} + i\omega\varepsilon_0 \quad \mathbf{E} = 0, \tag{1.4}$$

*in* $\mathbb{R}^3 \setminus \overline{\Omega}$*, where* $\Omega$ *is a bounded domain in* $\mathbb{R}^3$*.*
*The solutions* $\mathbf{E}, \mathbf{H}$*, are called radiating if they satisfy one of the following equivalent Silver-Müller radiation conditions*

$$\lim_{x\to\infty} (\mathbf{E} \times x + |x|\mathbf{H}) = 0,$$

$$\lim_{x\to\infty} (\mathbf{H} \times x - |x|\mathbf{E}) = 0,$$

*uniformly in all directions* $\frac{x}{|x|}$*, where* $r = |x|$*,* $x \in \mathbb{R}^3 \setminus \{0\}$*.*

## 1.2 The homogeneous Helmholtz equation

In this section, we introduce the connection between the Maxwell and the Helmholtz differential equation. Let $\Omega$ be a bounded domain in $\mathbb{R}^3$ with a regular boundary $\partial\Omega$. The permeability and permittivity are considered in the free space and thus supposed to be positive constants, namely $\mu_0$ and $\varepsilon_0$ respectively. We denote $C^1(\mathbb{R}^3 \setminus \overline{\Omega})$ and $C^2(\mathbb{R}^3 \setminus \overline{\Omega})$ to be the spaces of one-time and two-times continuously differentiable functions on $\mathbb{R}^3 \setminus \overline{\Omega}$ respectively. We suppose that the regular electromagnetic fields $\mathbf{E}, \mathbf{H} \in C^1(\mathbb{R}^3)$ are solutions of the Maxwell's equations

$$\nabla \times \mathbf{E} - i\omega\mu_0\mathbf{H} = -\mathbf{J}_m, \tag{1.5}$$

$$\nabla \times \mathbf{H} + i\omega\varepsilon_0\mathbf{E} = \mathbf{J}_e, \tag{1.6}$$

where $\mathbf{J}_m$ and $\mathbf{J}_e$ are given regular current fields on $\Omega$ with compact support in $\overline{\Omega}$ *i.e.*

$$\mathbf{J}_m(x) = \mathbf{J}_e(x) = 0 \text{ for } x \notin \overline{\Omega}.$$

We find that $\mathbf{E}, \mathbf{H} \in C^1(\mathbb{R}^3 \setminus \overline{\Omega})$ admit vanishing divergence fields on $\mathbb{R}^3 \setminus \overline{\Omega}$:

$$\nabla \cdot \mathbf{E} = 0, \tag{1.7}$$

$$\nabla \cdot \mathbf{H} = 0, \tag{1.8}$$

resulting from considering the homogeneous forms of equations (1.5),(1.6) together with the properties of the nabla operator, namely $\nabla \cdot \nabla \times \mathbf{E} = 0$ and $\nabla \cdot \nabla \times \mathbf{H} = 0$. If we further suppose that $\mathbf{E}, \mathbf{H}$ are two-times continuously differentiable functions on $\mathbb{R}^3 \setminus \overline{\Omega}$, namely $\mathbf{E}, \mathbf{H} \in C^2(\mathbb{R}^3 \setminus \overline{\Omega})$, then we take the curl of (1.5) on $\mathbb{R}^3 \setminus \overline{\Omega}$:

$$\nabla \times \nabla \times \mathbf{E} = i\omega\mu_0 \quad \nabla \times \mathbf{H}. \tag{1.9}$$

Substituting (1.6) in (1.9) gives

$$\nabla \times \nabla \times \mathbf{E} - \omega^2 \mu_0 \varepsilon_0 \quad \mathbf{E} = 0. \tag{1.10}$$

Equation (1.10) is called the vector wave equation. We can moreover use the identity

$$\nabla \times \nabla \times \mathbf{E} = -\Delta \mathbf{E} + \nabla(\nabla \cdot \mathbf{E}), \tag{1.11}$$

together with (1.7). By substituting them in (1.10), we get on $\mathbb{R}^3 \setminus \overline{\Omega}$ the vector Helmholtz equation for the electric field

$$\Delta \mathbf{E} + \omega^2 \varepsilon_0 \mu_0 \mathbf{E} = 0, \tag{1.12}$$

where $\Delta$ is the Laplacian. Similarly, we get the vector Helmholtz equation for the magnetic field, thus:

$$\Delta \mathbf{E} + \kappa^2 \mathbf{E} = 0, \tag{1.13}$$

$$\Delta \mathbf{H} + \kappa^2 \mathbf{H} = 0, \tag{1.14}$$

where $\kappa := \omega\sqrt{\varepsilon_0 \mu_0}$. The Maxwell's equations are then reduced to the Helmholtz equation in the case of divergence-free fields. Equations (1.13), (1.14) are true for each cartesian component of the electromagnetic fields. If we denote the magnitude of this component with $u$, then we get the scalar Helmholtz equation:

$$\Delta u + \kappa^2 u = 0 \tag{1.15}$$

From physical point of view, the solutions of the scalar Helmholtz equation must satisfy the Sommerfeld radiation condition. This condition specifies the appropriate geometric attenuation of a solution to the Helmholtz equation.

**Definition 1.3.** *Let $\kappa > 0$ and $\Omega$ be a bounded domain in $\mathbb{R}^3$. A solution $u \in C^2(\mathbb{R}^3 \setminus \overline{\Omega}, \mathbb{C})$ to the scalar Helmholtz equation*

$$\Delta u + \kappa^2 u = 0 \quad \text{in } \mathbb{R}^3 \setminus \overline{\Omega}, \tag{1.16}$$

*satisfies the Sommerfeld radiation condition if*

$$\lim_{r \to \infty} r \left( \frac{\partial u}{\partial r} - i\kappa u \right) = 0,$$

*uniformly in all directions $\frac{x}{|x|}$, where $r = |x|$, $x \in \mathbb{R}^3 \setminus \{0\}$.*

The fundamental solution $\Phi_\kappa^n$ of the Helmholtz equation $\Delta u + \kappa^2 u = 0$ in $\mathbb{R}^n, n \in \mathbb{N}$, which satisfies the Sommerfeld radiation condition, is given by

$$\Phi_\kappa^1(x) = \frac{i}{2\kappa}\, e^{i\kappa|x|} \qquad \text{for } x \in \mathbb{R} \setminus \{0\}.$$

$$\Phi_\kappa^2(x) = \frac{i}{4}\, H_0(\kappa|x|) \quad \text{for } x \in \mathbb{R}^2 \setminus \{0\},$$

$$\Phi_\kappa^3(x) = \frac{1}{4\pi}\frac{e^{i\kappa|x|}}{|x|} \qquad \text{for } x \in \mathbb{R}^3 \setminus \{0\},$$

where $H_0$ is the zero order Hankel function of the first kind, see, e.g., [8,30].

The *Green's function* associated with the Helmholtz operator $(\Delta + \kappa^2)$, $\kappa > 0$ and with the Sommerfeld radiation condition, is given by

$$g_\kappa^n(x,y) := \Phi_\kappa^n(x-y) \text{ for } x \neq y,\ x, y \in \mathbb{R}^n, n = 1,2,3. \tag{1.17}$$

# Chapter 2

# Mathematical Modeling

In this chapter we derive the mathematical modeling of the ARC. Based on the Maxwell's equations, we derive first a boundary value problem (BVP) to describe electromagnetic waves in a stratified medium [8]. The direct problem is concerned with determining of the electromagnetic field based on given coating refractive indices. Next, we derive an equivalent integral equation of Lippmann-Schwinger type by calculating the corresponding integral kernel. The direct problem of the model assigns the values of the electromagnetic fields. In practice, there is a physical possibility to measure these values. Moreover, there is a practical need to improve the quality of the coatings. This improvement is achievable by choosing the most appropriate refractive index. The best choice of the contrast function of the coating leads, in turn, to a more absorbed energy inside the coating. Dealing with such internal quantity requires solving the inverse problem of the model. Therefore, it is worth dealing with the inverse problem which determines the refractive index of the coating depending on the given values of the field. This will be done in Chapter 3. On the free surface of the coating, the boundary values are determined by the reflection coefficients which are the input data used for solving the inverse problem. Accomplishing true direct simulations on the boundary is useful for data generation. The accuracy of the data is crucial when solving the inverse problem.

## 2.1 Model as a boundary value problem

The theory of Maxwell, prescribed in the first chapter of this thesis, plays a key role in dealing with the light propagation and scattering in dielectric thin films. Depending on this theory, we describe the mathematical modeling of this physical electromagnetic phenomenon. We refer to Appendix (A) for details about the physics of Anti-Reflection Coatings. We consider the case of a normal incidence, namely the incident angle $\theta = 0$, since it proposes most of the related physics, see figure (2.1). For the case of an arbitrary

incident angle, we refer to [30].

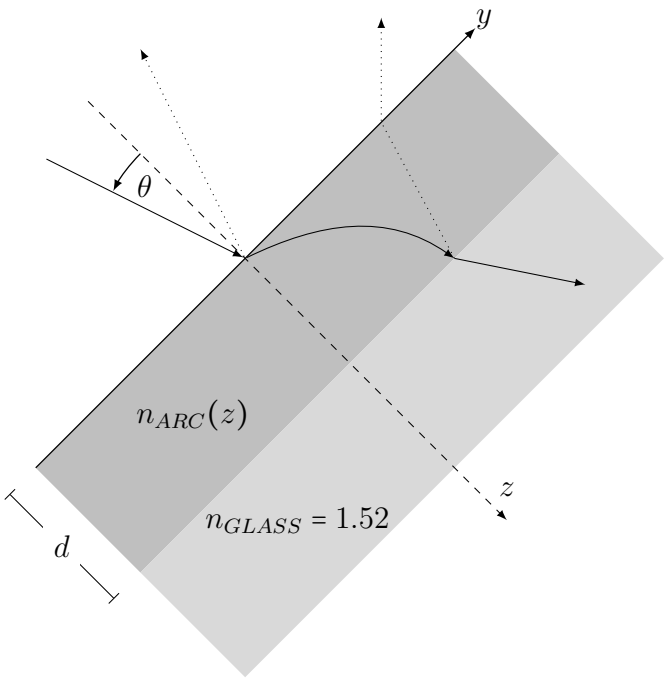


**Figure 2.1:** ARC in contact with a glass substrate

A medium is said to be stratified if the electromagnetic properties $\varepsilon$ and $\mu$ are constant throughout each plane perpendicular to a fixed direction [8], say $z$, it means

$$\varepsilon(x, y, z) = \varepsilon(z) \quad \text{and } \mu(x, y, z) = \mu(z)$$

We consider a plane time-harmonic wave propagating through a stratified nonmagnetic ($i.e.$, $\mu(z) = \mu_0$) medium. We suppose the electric wave to be linearly polarized in the direction perpendicular to the plane of incidence $i.e.$, a transverse electric wave (denoted by TE). An electromagnetic wave is said to be transverse magnetic (denoted by TM) when it is linearly polarized with its magnetic wave orthogonal to the plane of incidence. Since any plane wave with an arbitrary polarization may be decomposed into two waves, one is TE and the other is a TM wave, we may use the duality between the electric and the magnetic fields in the Maxwell's equations to deduce results on TM from corresponding results on TE, see [8].

We take the plane incidence to be $y, z$ plane where $z$ is the direction of stratification and of incidence.

For a TE wave, the polarization is along the $x$-direction, this means

$E_y = E_z = 0$. In this case the Maxwell's equation read

$$\nabla \times \mathbf{E} - i\omega\mu_0\mathbf{H} = 0, \tag{2.1}$$

$$\nabla \times \mathbf{H} + i\omega\varepsilon(z)\mathbf{E} = 0. \tag{2.2}$$

By using the properties of the nabla operator $\nabla = (\partial_x, \partial_y, \partial_z)^T$, equations (2.1), (2.2) become

$$\frac{\partial H_z}{\partial y} - \frac{\partial H_y}{\partial z} + i\omega\varepsilon(z)E_x = 0 \tag{2.3}$$

$$\frac{\partial H_x}{\partial z} - \frac{\partial H_z}{\partial x} = 0 \tag{2.4}$$

$$\frac{\partial H_y}{\partial x} - \frac{\partial H_x}{\partial y} = 0 \tag{2.5}$$

and

$$i\omega\mu_0 H_x = 0 \tag{2.6}$$

$$\frac{\partial E_x}{\partial z} - i\omega\mu_0 H_y = 0 \tag{2.7}$$

$$\frac{\partial E_x}{\partial y} + i\omega\mu_0 H_z = 0 \tag{2.8}$$

By taking the derivative of $H_y$ and $H_z$ in (2.7), (2.8) then substituting the values of $\frac{\partial H_y}{\partial z}$, $\frac{\partial H_z}{\partial y}$ in (2.3), we get

$$\frac{\partial^2 E_x}{\partial y^2} + \frac{\partial^2 E_x}{\partial z^2} + \omega^2\mu_0\varepsilon(z)E_x = 0$$

The coating space-dependent permittivity is given by

$$\varepsilon(z) = \varepsilon_0 n^2(z) = \varepsilon_0(1 + f(z)),$$

with $n(z)$ and $f(z)$ the refractive index and the contrast function of the coating respectively. We have the free space wave number $\kappa = \omega\sqrt{\mu_o\varepsilon_0}$. We further set the magnetic permeability $\mu_0 = 1$ since we have a nonmagnetic medium, we get

$$\frac{\partial^2 E_x}{\partial y^2} + \frac{\partial^2 E_x}{\partial z^2} + \kappa^2 n^2(z)E_x = 0.$$

Using a separation ansatz

$$E_x = v(y)u(z),$$

we get the differential system provided that the complex valued functions $u$ and $v$ do not vanish:

$$-\frac{v''(y)}{v(y)} = \frac{u''(z)}{u(z)} + \kappa^2\varepsilon(z),$$

where the left hand side depends on $y$ and the right hand side depends on $z$. It yields that there exists a positive constant for physically relevant solutions

$$\frac{v''(y)}{v(y)} = -a^2,$$

and

$$u''(z) + \kappa^2 n^2(z)u(z) = a^2 u(z).$$

Let $\alpha$ be such that $\alpha^2 = \frac{a^2}{\kappa^2}$, then

$$u''(z) + \kappa^2 \left(n^2(z) - \alpha^2\right) u(z) = 0. \tag{2.9}$$

It follows that

$$v(y) = v(0)(c_1 e^{i\kappa\alpha y} + c_2 e^{-i\kappa\alpha y}),$$

with the constants $c_1, c_2$. Consequently

$$E_x = u(z)(c_1 e^{i\kappa\alpha y} + c_2 e^{-i\kappa\alpha y}),$$

where the complex-valued function $u$, depending on $z$, satisfies the differential equation (2.9). We consider an incident wave $u_{inc}(z) = e^{i\kappa n_0 z}$, where $n_0$ is the refractive index of the air environment ($n_0 = 1$). The ARC has a given thickness $d$ and a refractive index $n_{ARC}(z) = n(z)$, in contact with a glass substrate of uniform refractive index $n_{Glass} = n_s = 1.52$. Let the interval $\Omega = (0, d) \in \mathbb{R}$ be the bounded domain of the relevant coating with the points $z = 0$ and $z = d$ as model boundaries. We consider only wave propagation in the $z-$direction, *i.e.*, we set $\alpha = 0$ in (2.9). Denoting the magnitude of $E_x$ with $u$, we get the scalar Helmholtz equation

$$u''(z) + \kappa^2 n^2(z)\ u(z) = 0, \quad z \in (0, d), \tag{2.10}$$

where $u''$ is the second derivative of $u$ with respect to the model variable $z$. Equation (2.10) represents our model in the coating's interval $(0, d)$.

For the sake of scaling into the interval $[0, 1]$, we replace $z$ with $z/d$ to obtain

$$u''(z) + \kappa^2 d^2 n^2(z)\ u(z) = 0, \quad z \in (0, 1). \tag{2.11}$$

If we denote with $\beta = \kappa d$ the nondimensionalised wave number, we get:

$$u''(z) + \beta^2 n^2(z)\ u(z) = 0, \quad z \in (0, 1). \tag{2.12}$$

Equation (2.12) is the second order differential Helmholtz equation with variable coefficient. It represents our model problem with the related boundary conditions.

### Boundary conditions

The second order differential Helmholtz equation (2.12) is endowed with conditions at the boundaries of the medium. These are generated by the continuity of the tangential components of electric and magnetic fields across the boundaries $z = 0$ and $z = 1$. The continuity at the upper interface of the slab ($z < 0$) implies that each tangential component of the electromagnetic fields is expressed as sum of the incident and reflected (scattered) fields, see (A.4), (A.5). The magnetic field $H$ is indicated by the gradient of the electric field $E$, check (2.7), (2.8). Thus, the continuity condition is reduced into the magnitudes of the electromagnetic field $u(0)$ together with its first derivative $u'(0)$. The solution $u(z)$ of equation (2.12) at $z < 0$ is a linear combination between the incident and reflected fields

$$u(z) = e^{in_0\beta z} + \mathcal{R}(\beta)e^{-in_0\beta z},\ z < 0.$$

The first derivative of $u(z)$ is given by

$$u'(z) = in_0\beta\ e^{in_0\beta z} - in_0\beta\ \mathcal{R}(\beta)e^{-in_0\beta z}\ z < 0,$$

where $\mathcal{R}(\beta)$ is called the *reflection coefficient*. Practically, the reflection coefficient can be measured for any value of $\beta$ which is ranging in some interval $[\beta_{\min}, \beta_{\max}]$. In the case of the inverse problem of our model, the varying of the wave number $\beta$ is motivated by the need of numerically solving the model problem. The model problem is reduced, after discretization, into solving a system of linear equations. To numerically solve this system, we have to vary the wave number.

By taking the values of $u(z)$,$u'(z)$ at $z = 0$ we obtain

$$u(0) = 1 + \mathcal{R}(\beta), \tag{2.13}$$

$$u'(0) = in_0\beta - in_0\beta\ \mathcal{R}(\beta). \tag{2.14}$$

It yields

$$u'(0) + in_0\beta\ u(0) = 2in_0\beta. \tag{2.15}$$

The continuity at the lower interface of the slab ($z > 1$) considers only the transmitted wave. Hence, the second boundary condition is similarly produced by taking the values of $u(1)$ and $u'(1)$. The solution $u(z)$ of equation (2.12) at $z > 1$ is given by

$$u(z) = \mathcal{T}(\beta)e^{-in_s\beta z},\ z > 1,$$

where $\mathcal{T}(\beta)$ is the *transmission coefficient*. The first derivative $u'(z)$ is given by

$$u'(z) = +in_s\beta\ \mathcal{T}(\beta)e^{in_s\beta z}.$$

We take the values of $u(z)$,$u'(z)$ at $z = 1$ to obtain

$$u(1) = \mathcal{T}(\beta)\ e^{in_s\beta}, \tag{2.16}$$

$$u'(1) = in_s\beta\ \mathcal{T}(\beta)\ e^{in_s\beta}. \tag{2.17}$$

The second boundary condition of our problem is obtained by solving equations (2.16),(2.17) as

$$u'(1) - in_s\beta\ u(1) = 0. \tag{2.18}$$

For formulas relating $R(\beta)$ and $T(\beta)$ to the refractive indices of the stratified interfaces, we refer to Appendix (A).

Considering the equation (2.12) in addition to the slab boundary conditions (2.15),(2.18) produces mainly our model as a boundary value problem:

$$(BVP)\begin{cases} u''(z) + \beta^2 u(z) = & -\beta^2 f(z)u(z),\ z \in (0,1), \\ u'(0) + in_0\beta\ u(0) = & 2in_0\beta, \\ u'(1) - in_s\beta u(1) = & 0. \end{cases} \tag{2.19}$$

In the direct problem, we are concerned with the determination of the scattered electromagnetic field for a given incident field impinging upon our medium with given electromagnetic properties, namely the given space-dependent refractive index of the coating. However, in the inverse problem, we have to determine the refractive index of the coating depending on the given incident and scattered fields which are represented by the reflection coefficients.

In section (2.2), we formulate the direct problem as an integral equation, in which the boundary conditions are already embedded.

## 2.2 Formulation of the direct problem as an integral equation

For solving the boundary value problem defined in (2.19), we formulate it as an equivalent integral equation. We recall the model equation as

$$u''(x) + \beta^2 u(x) = -\beta^2 f(x)u(x). \tag{2.20}$$

We split the total solution of equation (2.20) into a sum of an incident wave and a scattered wave

$$u(x) = u^0(x) + u^s(x), \tag{2.21}$$

where $u^0$ is a solution of the homogeneous Helmholtz equation

$$u''(x) + \beta^2 u(x) = 0. \tag{2.22}$$

A solution $u^0$ of (2.22) is given as (see, e.g., [28, 29])

$$u^0(x) = c_1 e^{i\beta x} + c_2 e^{-i\beta x}, \tag{2.23}$$

where the constants $c_1$ and $c_2$ must satisfy the boundary conditions in (2.19). After some calculations, we obtain

$$u^0(x) = e^{i\beta x} + \eta e^{-i\beta(x-2)}, \tag{2.24}$$

with $\eta := \frac{1-n_s}{1+n_s}$. Alternatively, the fundamental solution $u^0$ of (2.22) is given in terms of trigonometric functions as

$$u^0(x) = d_1 \cos(\beta x) + d_2 \sin(\beta x),$$

where the corresponding constants in this case are

$$d_1 = \frac{2i\cos\beta + 2n_s \sin\beta}{(1+n_s)\sin\beta + i(1+n_s)\cos\beta},$$

$$d_2 = i(2 - d_1).$$

The solution $u^s$ of the inhomogeneous Helmholtz equation (2.20), related to the model, is given by

$$u^s(x) = -\beta^2 \int_0^1 k_\beta(x,y) u(y) f(y) dy, \tag{2.25}$$

where $k_\beta(x,y)$ the corresponding integral kernel which is to be computed. If we substitute (2.24),(2.25) in equation (2.21) we obtain the total solution as

$$u(\beta, x) = -\int_0^1 \beta^2 k(\beta, x, y) f(y) u(\beta, y) dy + u^0(\beta, x). \tag{2.26}$$

For a given contrast function $f$ of the coating we get a Fredholm equation of the second kind with respect to the electromagnetic field $u$

$$u(\beta, x) + \int_0^1 k_f(\beta, x, y) u(y) dy = u^0(\beta, x), \quad x \in (0,1), \tag{2.27}$$

with the kernel:

$$k_f(\beta, x, y) = \beta^2 k(\beta, x, y) f(y).$$

Equation (2.27) is known in the scattering theory as Lippmann-Schwinger integral equation [13]. Formulating (2.27) using operator notation produces

$$\big(\mathcal{I} + K_f\big) u = u^0,$$

with the identity operator $\mathcal{I}$ and the integral operator $K_f$ given by:

$$K_f u(\beta, x) = \int_0^1 k_f(\beta, x, y) u(y) dy. \tag{2.28}$$

Thus, the direct problem is concerned with the determination of the total field $u$ from a given incident field $u^0$ and a given refractive index $n$ where $n^2 = 1 + f$.

For fixed wave number $\beta$, we set $k_\beta(x, y) = k(\beta, x, y)$. For calculating the integral kernel $k_\beta(x, y)$, we consider the elliptic differential operator of Helmholtz

$$Lu = (\Delta + \beta^2)u \tag{2.29}$$

defined on the space of twice differentiable functions. The computation of the integral kernel is classical [29]. We calculate the kernel using a constructive method.

**Theorem 2.2.1.** *Let the incident field $u^0$ be as in (2.24). Then, $u \in C^2((0,1)) \cap C^1([0,1])$ is solution of the BVP (2.19) iff*

$$u(x) = -\int_0^1 \beta^2 k_\beta(x, y) f(y) u(y) dy + u^0(x),$$

*with the integral kernel $k_\beta(x, y)$ given by*

$$k_\beta(x, y) = \begin{cases} \frac{1}{2i\beta} e^{-i\beta(x-y)} + \frac{\eta}{2i\beta} e^{-i\beta(x+y-2)} & \text{for} \quad x \leq y, \\ \frac{1}{2i\beta} e^{+i\beta(x-y)} + \frac{\eta}{2i\beta} e^{-i\beta(x+y-2)} & \text{for} \quad x > y. \end{cases} \tag{2.30}$$

*Proof.* We seek an integral operator $K$ with

$$Ku(x) = \int_0^1 k(x, y) u(y) dy \quad u \in L_2[0, 1] \tag{2.31}$$

defined on the space $L_2[0, 1]$ such that $Ku$ satisfies the boundary conditions and

$$LKu = u. \tag{2.32}$$

For $k$ to satisfy (2.32) we require that

$$\int_0^1 Lk(x, y) u(y) dy = u(x). \tag{2.33}$$

Thus, we seek a Green's function $k(x, y)$ such that

$$Lk(x, y) = 0, \quad x \neq y. \tag{2.34}$$

We solve the equation (2.34) subject to the homogeneous forms of the boundary conditions in (2.19). Let $k_1$ be solution to the initial value problem

$$k_1'' + \beta^2 k_1 = 0, \tag{2.35}$$
$$k_1'(0) + in_0\beta k_1(0) = 0. \tag{2.36}$$

Moreover, let $k_2$ be solution to the initial value problem

$$k_2'' + \beta^2 k_2 = 0, \tag{2.37}$$
$$k_2'(1) - in_s\beta k_2(1) = 0. \tag{2.38}$$

With $k'$ and $k''$ we denote the corresponding first and second partial derivatives of the kernel with respect to $x$. Equation (2.35) is the homogeneous Helmholtz equation and its solution is given as:

$$k_1(x) = c_1 e^{i\beta x} + c_2 e^{-i\beta x}.$$

By taking the first derivative with respect to $x$ we obtain

$$k_1'(x) = i\beta c_1 e^{i\beta x} - i\beta c_2 e^{-i\beta x}.$$

The boundary condition (2.36) implies that $c_1 = 0$ and the parameter $c_2$ can be assigned arbitrarily, we get

$$k_1(x) = c_2 e^{-i\beta x}.$$

Similarly, equation (2.37) is the homogeneous Helmholtz equation with the following solution and its first derivative

$$k_2(x) = c_3 e^{i\beta x} + c_4 e^{-i\beta x},$$
$$k_2'(x) = i\beta c_3 e^{i\beta x} - i\beta c_4 e^{-i\beta x}.$$

We do some calculations to obtain that

$$c_3 = \frac{c_4}{\eta} e^{-2i\beta},$$

and

$$k_2(x) = c_4 \left( \frac{1}{\eta} e^{i\beta(x-2)} + e^{-i\beta x} \right).$$

Now we write the kernel as

$$k(x,y) = \begin{cases} k_1(x)k_2(y) & \text{for} \quad x < y, \\ \\ k_2(x)k_1(y) & \text{for} \quad x > y. \end{cases}$$

We require that $k(x,y)$ be continuous at $x=y$, this means that

$$k_1(x)k_2(x) = k_2(x)k_1(x) \Rightarrow c_2 = c_4 = c,$$

and then

$$k(x,y) = c \begin{cases} k_1(x)k_2(y) & \text{for} \quad x < y, \\ \\ k_2(x)k_1(y) & \text{for} \quad x > y \end{cases} \tag{2.39}$$

In order to fix the constant $c$ we integrate equation (2.34) over $x$ in the interval $[y-\epsilon, y+\epsilon]$. To satisfy (2.33) we have

$$\int_{y-\epsilon}^{y+\epsilon} (k'' + \beta^2 k)dx = 1,$$

This leads to

$$\lim_{\varepsilon \to 0} \left[k'(y+\epsilon, y) - k'(y-\epsilon, y)\right] = 1. \tag{2.40}$$

We calculate the first partial derivative of $K(x,y)$ with respect to $x$ as

$$k'(x,y) = c \begin{cases} k_1'(x)k_2(y) & \text{for} \quad x < y, \\ \\ k_2'(x)k_1(y) & \text{for} \quad x > y. \end{cases}$$

For $x=y$, substituting the last in (2.40) produces:

$$c = \frac{1}{k_1(y)k_2'(y) - k_1'(y)k_2(y)},$$

after doing some calculations we obtain

$$c = \frac{\eta e^{2i\beta}}{2i\beta}.$$

substituting the value of $c$ in (2.39) and doing calculations we obtain the aimed integral kernel in the form

$$k_\beta(x,y) = \begin{cases} \frac{1}{2i\beta} e^{-i\beta(x-y)} + \frac{\eta}{2i\beta} e^{-i\beta(x+y-2)} & \text{for} \quad x \leq y, \\ \\ \frac{1}{2i\beta} e^{+i\beta(x-y)} + \frac{\eta}{2i\beta} e^{-i\beta(x+y-2)} & \text{for} \quad x > y. \end{cases} \tag{2.41}$$

After finding this kernel we easily check that it satisfies the Helmholtz equation and the corresponding boundary conditions. □

In Chapter 4, we use a quadrature method to solve the direct problem. For that purpose, we prepare a Matlab-code called *the direct solver*. This code computes the total field for a given contrast function. We use this direct solver to generate data required as an input for solving the inverse problem. The data are presented in the reflection coefficients which are the difference between the values of the incident and the total fields on the surface of the coating.

# Chapter 3

# The Inverse Problem and Methods of Solution

In this chapter, we investigate the inverse scattering problem of the model (2.19). The objective in this problem is to determine the spatially-varying refractive index based on the values of the reflection coefficients. Solving this problem consists of dealing with two major difficulties. The first is the nonlinearity; this is because of the nonlinear dependence of the field on the refractive index. The second is the ill-posedness. According to Hadamard, the existence, uniqueness, and stability of a solution are the three main conditions for the well-posedness of some linear or even nonlinear problem. If one of these conditions is not satisfied, then the problem is said to be ill-posed. Physically, regarding the existence of the solution, it is not necessary to find an ARC which fulfills a specific given range of the reflection coefficients. The non-uniqueness means that it is possible that different ARCs may produce the same range of the given reflection coefficients. Third concerning the instability, small errors in the reflection coefficients, lead to large errors in the contrast function which is the solution of this problem. This chapter proposes the regularization methods which are applied to stabilize the solution of both linearized and nonlinear inverse problems. We refer [1] mainly to [42,45] for a general analytic study of the regularization of ill-posed problems, besides [21, 55]. We formulate the inverse nonlinear problem of our model in Section 3.1. To deal with the nonlinearity, we consider an iterated Born approximation in Section 3.2. The second iteration of the Born approximation yields a quadratic approximation of the problem which is discussed also in the same section. Next, we introduce regularization methods including the AI-method to solve the linearized problem in Section 3.3. The last section of this chapter is devoted to dealing with the nonlinear problem of our model. For that purpose, we present an extension, introduced by Louis [43], of the AI-method for solving the quadratic problem.

[1] Both references [42] and [55] are in German language.

## 3.1 The inverse nonlinear scattering problem

In this work, we consider the inverse problem concerned with the determination of the optical coating refractive indices based on the values of the reflection coefficients which represent the input data. These reflection coefficients are the difference between total and incident fields at the surface of the coating. They are computed for different values of the wave numbers. We recall the boundary value problem (2.19) of our model:

$$(BVP)\begin{cases} u''(x)+\beta^2 u(x) = & -\beta^2 f(x)u(x),\ x\in(0,1), \\ u'(0)+in_0\beta\ u(0) = & 2in_0\beta, \\ u'(1)-in_s\beta u(1) = & 0. \end{cases} \tag{3.1}$$

If we consider the integral formulation (2.26), we obtain the total field as

$$u(x,\beta)=u^0(x,\beta)-\beta^2\int_0^1 k_\beta(x,y)u(y,\beta)f(y)dy, \text{ with } x,y\in[0,1]. \tag{3.2}$$

The electric field is measured at $x=0$. We get

$$\int_0^1 -\beta^2 k_\beta(0,y)u(y,\beta)f(y)dy=\underbrace{u(0,\beta)-u^0(0,\beta)}_{\text{Data}=:g(\beta)}, \tag{3.3}$$

which is a first kind integral equation. The kernel $k_\beta(0,y)$ is obtained from (2.30) as

$$k_\beta(0,y)=\frac{1}{2i\beta}\big(e^{i\beta y}+\eta e^{-i\beta y}e^{2i\beta}\big).$$

For a given field $u$ we have to find the unknown contrast function $f$, and then the refractive index $n^2=1+f$. This optical coating synthesis problem is an inverse medium scattering problem. Inverse scattering problems arise when information about some unknown object are recovered depending on measurements of waves scattered by this object. Such problems exist in diverse areas of applications as medical diagnostics, nondestructive industrial testing, submarine, and oil exploration. For more details about inverse scattering problems, we refer to [13]. One of the main difficulties in solving the inverse scattering problems is the nonlinearity. This is because the dependence of the field $u$ on the contrast function $f$ is nonlinear. The methods deal with nonlinearity vary between two approaches, the first one uses nonlinear techniques by applying *e.g.* iterative algorithms, consult Section (3.4) for details. Whereas, the second approach discusses linearized inversion schemes. The linearized schemes depend on approximations of Born or Rytov type [32, 53] which are valid for media with low contrasts, *e.g.*, [25]. We use Born approximation for linearizing the mathematical integral model (3.2).

## 3.2 Born series and approximations

We consider the integral formulation (3.2) of the BVP (3.1). In operator notation, it reads

$$u = u^0 + Afu, \tag{3.4}$$

where $A$ is the linear operator given by

$$A\varphi(x,\beta) = \int_0^1 -\beta^2 k_\beta(x,y)\varphi(y)dy = u(x,\beta) - u^0(x,\beta), \text{ with } \varphi = fu. \tag{3.5}$$

We denote by $A_f$ the operator defined as $A_f u = Afu$. Equation (3.4)reads as

$$u - A_f u = u^0,$$

$$\big[\mathcal{I} - A_f\big]u = u^0,$$

$$u = \big[\mathcal{I} - A_f\big]^{-1}u^0,$$

The operator $(\mathcal{I} - A_f)$ is supposed to be invertible in the vicinity of $f = 0$ and $(\mathcal{I}-A_f)^{-1}$ denoting the inverse operator of $(\mathcal{I}-A_f)$. We get the infinite Born series for the field $u$

$$u = \sum_{l=0}^{\infty} (A_f)^l u^0. \tag{3.6}$$

Thus, the Born series is an expansion of (3.4). The terms of this series represent the successively higher orders of the scattering [8]. If we just consider the first two orders in (3.6) and ignore the other higher orders, we obtain the finite Born series as

$$u(x,\beta) \approx \underbrace{u^0(x,\beta)}_{l=0} + \underbrace{A_f[u^0(y,\beta)]}_{l=1} + \underbrace{A_f\big[A_f[u^0(y,\beta)]\big]}_{l=2}, \tag{3.7}$$

here $l = 1$ and $l = 2$ stand for the Born Approximation for the field $u$ of the first-order and of the second-order, respectively. The electric field is measured at the point $x = 0$. We substitute that in (3.7) to obtain

$$\underbrace{A_f[u^0(y,\beta)](\beta)}_{A \text{ linearized } (A_1)} + \underbrace{A_f\big[A_f[u^0(y,\beta)]\big](\beta)}_{A \text{ quadratic } (A_2)} \approx \underbrace{u(0,\beta) - u^0(0,\beta)}_{=g(\beta) \text{ (Data)}}. \tag{3.8}$$

Equation (3.8) stands for the iterated Born approximation with regards to the field $u$.

### 3.2.1 The linear approximation

Here we are concerned with the case $l = 1$ in (3.7). Thus, we linearize the problem using the first-order Born approximation. The scattered field $u^s$ is supposed to be much smaller than the incident field $u^0$. Therefore, it could be neglected in (2.21) by setting

$$u(y, \beta) \approx u^0(y, \beta). \tag{3.9}$$

By substituting (3.9) in the left hand side of (3.3) we obtain the linear Fredholm integral equation of the first kind

$$\int_0^1 \underbrace{-\beta^2 k_\beta(0, y)u^0(y, \beta)}_{=:\tilde{k}(\beta,y)} f(y)dy = \underbrace{u(0, \beta) - u^0(0, \beta)}_{=:g(\beta)}. \tag{3.10}$$

We formulate equation (3.10) using operator notation, we obtain:

$$\begin{aligned} &A_1 : X = L_2([0, 1]) \longrightarrow L_2([\beta_{\min}, \beta_{\max}]) = Y, \\ &A_1 f(\beta) = \int_0^1 \tilde{k}(\beta, y)f(y)dy = g(\beta),\ y \in [0, 1] \end{aligned} \tag{3.11}$$

where $A_1$ is the linearized operator and $\tilde{k}(\beta, y)$ is the integral kernel given by

$$\tilde{k}(\beta, y) = \frac{\beta i}{2}\left(e^{2i\beta y} + \eta^2 e^{-2i\beta(y-2)} + 2\eta e^{2i\beta}\right). \tag{3.12}$$

The data are the differences between the values of the total and incident fields at the point $x = 0$. These differences are called the reflection coefficients. From these data, we have to find the unknown contrast function $f$ and, respectively the refractive index $n = \sqrt{1 + f}$. To numerically solve this inverse problem, we seek a system of linear equations. This requires a diversity of the wave number $\beta$. The diversity enables the descretization, and then, the reduction of this problem into a system of linear equations. According to [27, 40]; there is no unique solution to the inverse scattering problem neither linearized nor normalized, for a single frequency. The nondimensionalised wave number $\beta$ is ranging in the interval $[\beta_{\min}, \beta_{\max}]$. Hence, our linearized semi-discrete problem seeks $f$ as a solution of the equation:

$$A_1 f(\beta_j) = g(\beta_j) \qquad j = 1, ...., M, \tag{3.13}$$

where $\beta_j$ are samplings of the wave numbers.

The Born Approximation is a practically feasible linearizing method. The validity of this method is ensured when the contrast function $f$ satisfies the inequality

$$\kappa d \sup_{x\in(0,1)} |f(x)| < 4\pi b, \tag{3.14}$$

where $b$ is a small constant, in practice we take $b = 0.16$, see, e.g., [53]. The left hand side of this inequality is a rough estimate for the phase shift between the incident field and the wave propagation throughout the object. The range of the wave numbers $[\beta_{min}, \beta_{max}]$ taken in the numerical test examples must satisfy the condition above in order to get a good reconstruction.

### 3.2.2 The quadratic approximation

The quadratic approximation of the inverse problem discusses the case where $l = 2$ in (3.7). This comes as an additional step to improve the linear approximation. We have

$$\begin{aligned} A_2 f(\beta) &= A_1 f\big[A_1 f[u^0]\big](\beta) = A_1 f\big[-\beta^2 \int_0^1 k(y_1,\beta) u^0(y_1,\beta) f(y_1) dy_1\big] \\ &= -\beta^2 \int_0^1 k(y_2,\beta)\big[-\beta^2 \int_0^1 k_\beta(y_1,y_2) u^0(y_1,\beta) f(y_1) dy_1\big] f(y_2) dy_2 \\ &= \int_0^1 \int_0^1 \underbrace{\big[\beta^4 k(y_2,\beta) k_\beta(y_1,y_2) u^0(y_1,\beta)\big]}_{k^2_\beta(y_1,y_2)} f(y_1) f(y_2) dy_1 dy_2. \end{aligned} \tag{3.15}$$

Thus, the quadratic operator of our model is defined as

$$A_2 f(\beta) = \int_0^1 \int_0^1 k^2_\beta(y_1,y_2) f(y_1) f(y_2) dy_1 dy_2. \tag{3.16}$$

We compute next the integral kernel $k^2_\beta(y_1,y_2)$ of this quadratic operator. By changing the variables in (2.41), we obtain the integral kernel $k_\beta(y_1,y_2)$ as:

$$k_\beta(y_1,y_2) = \begin{cases} \frac{1}{2i\beta} e^{-i\beta(y_1-y_2)} + \frac{\eta}{2i\beta} e^{-i\beta(y_1+y_2-2)} & \text{for} \quad y_1 \le y_2, \\ \frac{1}{2i\beta} e^{+i\beta(y_1-y_2)} + \frac{\eta}{2i\beta} e^{-i\beta(y_1+y_2-2)} & \text{for} \quad y_1 > y_2. \end{cases} \tag{3.17}$$

From equation (2.24), we have

$$u^0(y_1,\beta) = e^{i\beta y_1} + \eta e^{-i\beta(y_1-2)}. \tag{3.18}$$

We refer to [8, 32] for more details about the Born approximation.

## 3.3 Regularization methods for linear problems

After linearizing the nonlinear inverse problem (3.3) in the last section, we still have to deal with the ill-posedness of the new linearized inverse scattering problem (3.11). The ill-posedness means that the solution of this problem may not exist. This solution, if it exists, may not be unique. Moreover, the dependence of this solution on the data is discontinuous. This ill-posedness occurs since the underlying operator is a compact operator with non-closed range defined between two Hilbert spaces. To stabilize the solution of our linearized inverse problem, we need to apply regularization methods. Famous regularization methods are truncated singular value decomposition, Tikhonov-Phillips methods, and the method of the Approximate Inverse.

If we consider a bounded linear operator $A$ between the Hilbert spaces $X$ and $Y$ with the norm $\| x \| = < x, x >$, where $< x, x >$ is the scalar product. Then according to the famous concept of Hadamard, the problem $(A, X, Y)$ of solving the equation $Af = g$ is called well posed if there exists a unique and a stable solution $f \in X$ for every data $g \in Y$. Otherwise the problem is called ill-posed. The stability of the solution is here in the sense that the operator $A$ has a continuous inverse. The problem is then ill-posed if the solution does not depend continuously on the data, *i.e.*, a small error in the data may produce a large error in the solution. This data noise is unavoidable and typical in practice since the measurements are endowed with errors. The integral equations of the first kind lead to compact operators with a non-closed range $\mathcal{R}(A)$ between two Hilbert spaces. The problem $(A, X, Y)$ is thus ill-posed since the pseudoinverse or the generalized inverse $A^\dagger$ of a linear operator $A$ is not continuous. The operator $A^\dagger$, named also *Moore-Penrose inverse*, with the domain $\mathcal{D}(A^\dagger) := \mathcal{R}(A) \oplus \mathcal{R}(A)^\perp$ is defined as [42]:

**Definition 3.1.** *If we consider the problem $(A, X, Y)$ then the generalized inverse of the linear operator $A$ is defined as*

$$\begin{aligned} A^\dagger : \mathcal{D}(A^\dagger) \subset \overline{\mathcal{R}(A)} \oplus \mathcal{N}(A^*) = Y &\longrightarrow \mathcal{N}(A)^\perp \subset X, \\ g &\longrightarrow f^\dagger, \end{aligned} \tag{3.19}$$

*where $\mathcal{N}(A^*)$ is the null-space of the adjoint operator $A^*$ of $A$, $\mathcal{N}(A)^\perp$ is the orthogonal complement of the null-space of $A$ and $f^\dagger$ is the minimum norm solution which minimizes the residual:*

$$J(f^\dagger; g) = \| Af^\dagger - g \| \leq \| Af - g \| \quad \forall f \in X.$$

Any compact operator $A$ between the Hilbert spaces $X$ and $Y$ admits a singular value decomposition $\{v_n, u_n; \sigma_n\}_n$, $n \in \mathbb{N}$ where $v_n$, $u_n$ are normalized and

$$Av_n = \sigma_n u_n \quad \text{and} \quad A^* u_n = \sigma_n v_n.$$

**Theorem 3.3.1.** *Let $A$ be a compact operator with the singular system $\{v_n, u_n; \sigma_n\}_n$. Then we have*

$$A^\dagger g = \sum_{\sigma_n > 0} \sigma_n^{-1} < g, u_n > v_n \quad for \quad g \in \mathcal{D}(A^\dagger).$$

*Proof.* We refer to [42, Chapter 3]. □

The regularization methods are used to stabilize the solution, e.g., [36], [37], [38]. The aim is to approximate the unbounded operator $A^\dagger$ with a family of continuous operators $T_\gamma$ as explained in the following definition.

**Definition 3.2.** *Let $A$ be a compact operator between the Hilbert spaces $X$ and $Y$, a regularization $\{T_\gamma\}_{\gamma>0}$ of $A^\dagger$ is a family of continuous operators $T_\gamma : Y \to X$ such that there exists a mapping*

$$\gamma : \mathbb{R}_+ \times Y \to \mathbb{R}_+$$

*called a regularization parameter satisfying*

$$\lim_{\epsilon \to 0} T_{\gamma(\epsilon, g^\epsilon)} g^\epsilon = A^\dagger g \tag{3.20}$$

*for every $g \in \mathcal{D}(A^\dagger) := \mathcal{R}(A) \oplus \mathcal{R}(A)^\perp$ and $g^\varepsilon \in Y$ with $\|g - g^\varepsilon\| \leq \varepsilon$.*
*If $T_\gamma$ are linear, then $\{T_\gamma\}_{\gamma>0}$ is called linear regularization.*

To evaluate the total error of solving an inverse problem we compare $A^\dagger$ and $T_\gamma$ with respect to the $L_2$-norm in (3.20), we obtain

$$\begin{aligned} \| T_\gamma g^\epsilon - A^\dagger g \| \leq & \| T_\gamma g^\epsilon - T_\gamma g + T_\gamma g - A^\dagger g \| \\ \leq & \| T_\gamma \| \underbrace{\| g^\epsilon - g \|}_{\text{Data Error}} + \underbrace{\| T_\gamma - A^\dagger \|}_{\text{Approximation Error}} \| g \| . \end{aligned} \tag{3.21}$$

If $\gamma$ is very small, the approximation error will be very small too. In this situation, $T_\gamma$ tends to $A^\dagger$ which is unbounded, a condition which is undesirable. The discretization leads to a numerically ill-conditioned system of equations. For large $\gamma$, the system tends to be well conditioned, however, $T^\gamma$ will go far away from $A^\dagger$. Thus, $T^\gamma$ is no more a good approximation of $A^\dagger$. As a result, the regularization parameter $\gamma$ is chosen optimally as a trade-off in order to keep the total error as small as possible. In our numerical simulation, $\gamma$ is chosen based on trial and error.

In our numerical simulation in Chapter 4, we apply the method of Approximate Inverse as a main regularization method for solving the inverse problem. This method is introduced sections (3.3.1) and (3.4.1) for both cases of linearized and quadratic problems, respectively. Moreover, we compare our numerical results in the case of the linearized problem with the

classical method of Tikhonov-Phillips. This method replaces minimizing $\| Af - g \|_Y$ by minimizing the cost functional

$$J_\gamma(f) := \| Af - g \|_Y^2 + \gamma^2 \| f \|_X^2, \tag{3.22}$$

with the penalty term $\gamma^2 \| f \|^2$ where $\| . \|$ is the $L_2$-norm. The functional $J_\gamma(f)$ admits a unique minimizer $f_\gamma \in X$ computed as the solution of the normal equation:

$$A^*Af^\gamma = A^*g,$$

$$A^*Af^\gamma + \gamma f^\gamma = A^*g, \tag{3.23}$$

$$(A^*A + \gamma\mathcal{I})f^\gamma = A^*g,$$

where $\mathcal{I}$ is the identity operator, $A^*$ is the adjoint operator of $A$ and $\gamma > 0$ is the regularization parameter. Finding the solution $f^\gamma$ is then reduced to numerically solving a system of linear equations with respect to the discretization of the aforementioned regularized normal equation (3.23). For more details, we refer mainly to [42, Chapter 4.2]. As an efficient and stable scheme, we next introduce the method of the Approximate Inverse for solving the linearized problem.

### 3.3.1 Approximate Inverse for the linearized problem

In order to stabilize the solution of our ill-posed linearized problem (3.11), we mainly use the method of the Approximate Inverse (AI). This method was firstly introduced in [48]. For the analytic study of this regularization method we refer to Louis [43]. AI is efficient method for solving linear problems [45] and nonlinear problems [43, 44] and later on in subsection (3.4.1). It has been extended for image reconstruction [46], for feature reconstruction [47], and for solving inverse problems on Banach-spaces [35, 58]. This method has been implemented successfully in many applications [1, 23, 24, 34, 36, 56, 59].

We consider a compact linear operator $A$, the aim of this method is to find a stable solution $f$ to the equation $Af = g$ by computing an approximation

$$f_\gamma(x) = \langle f, \delta_x^\gamma \rangle_X \quad \text{with} \quad \delta_x^\gamma \approx \delta_x.$$

The mollifier $\delta_x^\gamma$ converges (as $\gamma$ tends to zero) to the Delta distribution $\delta_x$ for the reconstruction point $x$. Let $n, m \in \mathbb{N}, \Omega \subset \mathbb{R}^n$ and let $X, Y$ be Hilbert spaces with $X = L_2(\Omega)^n$, let also $L(X, Y)$ be the space of linear continuous operators between $X$ and $Y$ and $L(X) = L(X, X)$. Then, we can introduce the following definition.

**Definition 3.3.** *The family of operators* $\{M_\gamma\}_{\gamma>0} \subset L(X)$ *forms an approximation of the identity if*

$$\lim_{\gamma\to 0} M_\gamma f = f \quad \text{for } f \in X.$$

$\{M_\gamma\}_{\gamma>0}$ *has the rate* $\alpha > 0$ *if there exist a positive constant* $C > 0$ *such that*

$$\| M_\gamma f - f \| \leq C\gamma^\alpha \| f \| \quad \text{for } f \in X.$$

*If furthermore for* $x \in \Omega$*, there exists* $\delta_x^\gamma \in X$ *such that for* $f \in X$

$$M_\gamma f(x) = < f, \delta_x^\gamma >, \quad x \in \Omega,$$

*then the function* $\delta^\gamma$ *defined by*

$$\delta^\gamma(x, y) := \delta_x^\gamma \text{ for } x, y \in \Omega$$

*is called the mollifier associated to* $M_\gamma$*.*

A typical example is the Gaussian mollifier given by

$$\delta^\gamma(x, y) = (2\pi)^{-n/2}\gamma^{-n} \exp(-| x - y |^2/(2\gamma^2)) \tag{3.24}$$

Some other example is the band-limiting filter

$$\delta^\gamma(x, y) = \left(\frac{\gamma}{\pi}\right)^n \operatorname{sinc}(\gamma(x - y)).$$

In both examples $\gamma$ acts as a regularization parameter. To relate the data $g$ to the solution we have to determine a reconstruction kernel $\psi_x^\gamma$ by solving the following auxiliary equation

$$A^*\psi_x^\gamma = \delta_x^\gamma, \tag{3.25}$$

where $\delta_x^\gamma$ is the mollifier defined above and $A^*$ is the adjoint operator of $A$. If equation 3.25 is not solvable then the reconstruction kernel $\psi_x^\gamma$ is approximated by minimizing the defect $\| A^*\psi^\gamma - \delta^\gamma \|$ which leads to the normal equation of 3.25 as

$$AA^*\psi_x^\gamma = A\delta_x^\gamma. \tag{3.26}$$

Then, depending on (3.25), it holds

$$\begin{aligned} f_\gamma(x) &= \langle f, \delta_x^\gamma \rangle_X \\ &= \langle f, A^*\psi_x^\gamma \rangle_X \\ &= \langle Af, \psi_x^\gamma \rangle_Y \\ &= \langle g, \psi_x^\gamma \rangle_Y =: S_\gamma g(x). \end{aligned} \tag{3.27}$$

For the case of (3.26), we have

$$\begin{aligned} f_\gamma(x) &= \langle f, \delta_x^\gamma \rangle_X \\ &\simeq \langle f, A^* \psi_x^\gamma \rangle_X \\ &= \langle Af, \psi_x^\gamma \rangle_Y \\ &= \langle g, \psi_x^\gamma \rangle_Y =: S_\gamma g(x). \end{aligned} \tag{3.28}$$

**Definition 3.4.** *Let $\delta_x^\gamma$ be a suitable mollifier and let $\psi_x^\gamma$ be the solution of (3.26), then $S_\gamma g := \langle g, \psi_x^\gamma \rangle$ is called the* ***approximate inverse*** *of the operator $A$ and $\psi_x^\gamma$ is called the* ***reconstruction kernel****.*

The minimum-norm solution of the equation $Af = g$ is the solution with the smallest norm. It lies in the range of the adjoint operator $A^*$ and then it is computed by solving the equation

$$AA^* u = g \quad \text{where} \quad f^\dagger = A^* u. \tag{3.29}$$

The next theorem [43] states the relation between the minimum norm solution $f^\dagger$ and the approximate inverse

**Theorem 3.3.2.** *The approximate inverse maps the right hand side of the equation $Af = g$ to the mollified version of the minimum norm solution $f_M$, i.e.,*

$$S_\gamma g = \langle f^\dagger, \delta_\gamma \rangle.$$

*Proof.* From (3.29) and depending on the injectivity of $AA^*$, we write

$$f^\dagger = A^*(AA^*)^{-1} g. \tag{3.30}$$

From (3.26) we obtain

$$\psi_x^\gamma = (AA^*)^{-1} A \delta_x^\gamma. \tag{3.31}$$

Thus, we find

$$\begin{aligned} S_\gamma g(x) &= \langle g, \psi_x^\gamma \rangle_Y \\ &= \langle g, (AA^*)^{-1} A \delta_x^\gamma \rangle_Y && \text{from (3.31)} \\ &= \langle A^*(AA^*)^{-1} g, \delta_x^\gamma \rangle_X && \text{Def. of } A^* \\ &= \langle f^\dagger, \delta_x^\gamma \rangle_X && \text{from (3.30).} \end{aligned}$$

□

The method of the approximate inverse is then stable since the reconstruction kernel $\psi_x^\gamma$ is precomputed independently from the data $g$ and the related measurement errors. Some other advantage of this method is the

flexibility in the choice of the mollifier $\delta_x^\gamma$ appropriately to the problem. We may also mention that this method is efficient taking in consideration how the invariance properties compute the reconstruction kernel with less numerical computation effort. Since it suffices, in the case of invariance, to compute the reconstruction kernel $\psi_x^\gamma$ at few, instead of all, reconstruction points $x$ in the underlying interval. For more details about the invariance we may refer to [43].

### Application of the Approximate Inverse

We recall now the linearized operator (3.11) of our model

$$\begin{aligned} A_1 : X = L_2([0,1]) &\longrightarrow L_2([\beta_{\min}, \beta_{\max}]) = Y, \\ A_1 f(\beta) &= \int_0^1 \tilde{k}(y,\beta) f(y) dy = g(\beta), \end{aligned} \tag{3.32}$$

where the related integral kernel (3.12) is

$$\tilde{k}(y,\beta) = \frac{\beta i}{2}\left(e^{2i\beta y} + \eta^2 e^{-2i\beta(y-2)} + 2\eta e^{2i\beta}\right). \tag{3.33}$$

Thus, the adjoint operator of $A$ is given by

$$\begin{aligned} A_1^* : L_2([\beta_{\min}, \beta_{\max}]) &\longrightarrow L_2([0,1]), \\ (A_1^* g)(y) &= \int_{\beta_{\min}}^{\beta_{\max}} \tilde{k}^*(y,\beta) g(\beta) d\beta, \quad y \in [0,1]. \end{aligned} \tag{3.34}$$

Applying the adjoint operator on the reconstruction kernel we get the auxiliary equation in the following integral form

$$(A_1^* \psi_x^\gamma)(y) = \int_{\beta_{\min}}^{\beta_{\max}} \tilde{k}^*(y,\beta) \psi_x^\gamma(\beta) d\beta = \delta_x^\gamma(y), \quad y \in [0,1], \tag{3.35}$$

where the integral kernel of $A^*$ is computed by

$$\tilde{k}^*(y,\beta) = \overline{\tilde{k}(y,\beta)} = \frac{-\beta i}{2}\left(e^{-2i\beta y} + \eta^2 e^{2i\beta(y-2)} + 2\eta e^{-2i\beta}\right). \tag{3.36}$$

By discretizing the interval $[\beta_{\min}, \beta_{\max}]$, the space $Y$ in (3.32) is replaced by the euclidean space $\mathbb{R}^M$. $M$ denotes the number of the wave lengths $\lambda_j, j = 1, ....., M$ taken in the interval $[\lambda_{\min}, \lambda_{\max}]$. Thus we have now $\beta_j$ with $1 \leq j \leq M$ such that

$$\beta_1 = \beta_{\min} = \frac{2\pi d}{\lambda_{\max}} \quad \text{and} \quad \beta_M = \beta_{\max} = \frac{2\pi d}{\lambda_{\min}}. \tag{3.37}$$

Depending on this discretization, the matrix that represents $A_1A_1^*$ is called the *Gram matrix*. We find the Gram matrix by setting

$$A_1A_1^* : L_2([\beta_{\min}, \beta_{\max}]) \longrightarrow L_2([\beta_{\min}, \beta_{\max}]),$$

where

$$\begin{aligned} A_1A_1^*g(\beta) &= \int_0^1 \tilde{k}(y,\beta) \underbrace{A_1^*g(y)}_{3.34} dy \\ &= \int_0^1 \tilde{k}(y,\beta) \left[ \int_{\beta_{\min}}^{\beta_{\max}} \tilde{k}^*(y,\beta')g(\beta')d\beta' \right] dy \\ &= \int_{\beta_{\min}}^{\beta_{\max}} \underbrace{\left[ \int_0^1 \tilde{k}(y,\beta)\tilde{k}^*(y,\beta')dy \right]}_{\textbf{Gram Matrix}} g(\beta')d\beta', \quad \text{for} \quad \beta, \beta^{'} \in [\beta_{\min}, \beta_{\max}]. \end{aligned} \tag{3.38}$$

Thus, the Gram matrix denoted by $G$ is given by

$$G_{\beta\beta'} = \int_0^1 \tilde{k}(y,\beta)\tilde{k}^*(y,\beta')dy, \quad \text{for} \quad \beta, \beta^{'} \in [\beta_{\min}, \beta_{\max}]$$

The analytical computation of the Gram matrix of our model for the case $\beta \neq \beta'$ is given by

$$\begin{aligned} G_{\beta\beta'} &= \beta\beta' \left[ \frac{e^{2i(\beta-\beta')} - 1}{8i(\beta-\beta')} + \frac{\eta^2 e^{-4i\beta'} \left[ e^{2i(\beta+\beta')} - 1 \right]}{8i(\beta+\beta')} + \frac{\eta e^{-2i\beta'} \left[ e^{2i\beta} - 1 \right]}{4i\beta} \right] \\ &- \beta\beta' \left[ \frac{\eta^2 e^{4i\beta} \left[ e^{-2i(\beta+\beta')} - 1 \right]}{8i(\beta+\beta')} + \frac{\eta^4 e^{4i(\beta-\beta')} \left[ e^{-2i(\beta-\beta')} - 1 \right]}{8i(\beta-\beta')} \right] \\ &- \beta\beta' \left[ \frac{\eta^3 e^{2i(2\beta-\beta')} \left[ e^{-2i\beta} - 1 \right]}{4i\beta} + \frac{\eta e^{2i\beta} \left[ e^{-2i\beta'} - 1 \right]}{4i\beta'} \right] \\ &+ \beta\beta' \left[ \frac{\eta^3 e^{2i(\beta-2\beta')} \left[ e^{2i\beta'} - 1 \right]}{4i\beta'} + \eta^2 e^{2i(\beta-\beta')} \right]. \end{aligned} \tag{3.39}$$

The wave numbers $\beta, \beta^{'}$ are ranging in the interval $[\beta_{\min}, \beta_{\max}]$.

The Gram matrix is computed for the case of $\beta = \beta'$ as

$$G_{\beta\beta} = \beta^2 \left[ \frac{(\eta^2+1)^2}{4} + \frac{\eta^2}{2} \right] + \eta\beta \left[ \frac{(\eta^2+1)}{2} \sin 2\beta + \frac{\eta}{8} \sin 4\beta \right]. \quad (3.40)$$

Similar to the discrete system of equations in (3.35), the Gram matrix is ill-conditioned. Therefore, we compute the reconstruction kernel numerically using the method of Tikhonov-Phillips

$$(\underbrace{A_1 A_1^*}_{G} + \gamma \mathcal{I}) \quad \psi_x^\gamma = A_1 \delta_x^\gamma.$$

Thus, the numerical implementation of the Approximate Inverse on our model deals with two regularization parameters. Another use of the Gram matrix is considered within the quadratic approximation of the problem as explained in the next section. The numerical implementation of this method is discussed in Chapter (4).

## 3.4 Regularization methods for nonlinear problems

The linearization methods, such as the previously introduced Born approximation, have a limited scope of application. This is because of their restricted validity (3.14). Therefor, in many applications it is necessary to treat the nonlinear model. The theory of linear ill-posed problems is rather completely developed [42,45]. This, however, is not the case for the nonlinear ill-posed problems.

Among the well-known methods for solving nonlinear inverse problems are the iterative schemes. These schemes reconstruct the unknowns of the problem iteratively from an *a priori* guess. The method of Tikhonov-Phillips is reformulated to solve nonlinear problems in the sense of least squares. To briefly explain that, we consider a nonlinear operator equation of the form

$$\mathcal{A}(f) = g,$$

where $\mathcal{A} : X \longrightarrow Y$ is a continuous nonlinear operator. Recalling the Tikhonov-Phillips minimizer described in equation (3.22) for solving the linearized problem

$$J_\gamma(f) := \| Af - g \|_Y^2 + \gamma^2 \| f \|_X^2 . \quad (3.41)$$

A generalization of the functional (3.41) to the nonlinear case is given by

$$\mathcal{J}_\gamma(f) := \| \mathcal{A}(f) - g \|_Y^2 + \gamma^2 \| f - f^* \|_X^2, \quad (3.42)$$

where $f^* \in X$ is an *a priori* guess of the solution $f$ and $\gamma^2 \| f - f^* \|^2$ is the penalty regularization term. For more details, the reader is advised

to consult [21, Chapter 10] and [55, Chapter 7]. The iteration methods are typically used to solve a sequence of forward problems via, *e.g.*, finite difference schemes as done in [41], where a similar generalization to (3.42) was used to solve the inverse nonlinear problem of the BVP (3.1). We refer to [21, Chapter 11] for other iterative methods including Landweber method and Gauss-Newton-type methods.

Other schemes such as [7, 57] solve the nonlinear inverse problem of (3.1) by using coupled-mode Zakharov-Shabat systems. Theses methods are applied after a reduction of the second order Helmholtz equation into a system of first order differential equations. Such systems are solved, in most cases, numerically. We refer also to [12] for methods based on trace formula, and for [19] for methods that use spline approximation projection.

We use in this work a direct method to solve the nonlinear inverse problem. The framework for this approach was introduced in [60, 61]. An algorithmic realization using the Approximate Inverse is due to Louis [43]. In this approach, the Born series is firstly expressed as a formal power series in tensor powers of the searched-for quantity. After that, this quantity, which is the solution of the inverse problem, is formulated explicitly as an inverse Born series in tensor powers of the scattering data. This method reduces the ill-posed nonlinear problem into multilinear problems with successive orders. The first problem is an ill-posed linear equation resulting from considering the first order in the inverse Born series. Whereas, the multilinear problems of higher orders are obtained by power series identification. For application of this approach to solve nonlinear inverse scattering problems in optical tomography, see [50, 51].

In our research, we solve the inverse nonlinear problem described in equation (3.3) by considering only the first two orders of the forward Born series (3.6). The regularization method used is due to Louis [43, 44] who extended the method of the Approximate Inverse to calculate a quadratic approximation to the solution of the nonlinear problem.

### 3.4.1 Approximate Inverse for the quadratic problem

In [43], Louis extended the method of the Approximate Inverse for solving some nonlinear problems successfully. For simplicity, we consider the quadratic problem which coincides with the finite Born series (3.7), see Section (3.2.2). We directly apply the approach on our model as follows. Consider the nonlinear operator

$$\mathcal{A} : X = L_2([0,1]) \longrightarrow L_2([\beta_{min}, \beta_{max}]) = Y, \tag{3.43}$$

Suppose that, the interval $[\beta_{\min}, \beta_{\max}]$ is descretized, then the co-domain of operator $\mathcal{A}$ in (3.43) is replaced by the euclidean space $\mathbb{R}^M$. Here $M$ denotes the number of the wave numbers $\beta_j,\ 1 \leq j \leq M$ chosen in the

interval $[\beta_{\min}, \beta_{\max}]$. We suppose further, that the nonlinear operator $\mathcal{A}$ is splitted as

$$\mathcal{A}f = A_1 f + A_2 f, \tag{3.44}$$

where $A_1$ is the linear operator (3.11) of our model, given as

$$(A_1 f)_{\beta_j} = \int_0^1 \tilde{k}^1_{\beta_j}(y) f(y) dy, \qquad j = 1, ...., M,$$

with the corresponding integral kernel, recall (3.12)

$$\tilde{k}^1_{\beta_j}(y) = \frac{-\beta_j}{2i}\left(e^{2i\beta_j y} + \eta^2 e^{-2i\beta_j(y-2)} + 2\eta e^{2i\beta_j}\right),$$

and $A_2$ is the quadratic operator (3.16) defined as

$$(A_2 f)_{\beta_j} = \int_0^1 \int_0^1 k^2_{\beta_j}(y_1, y_2) f(y_1) f(y_2) dy_1 dy_2,$$

where $y_1$ and $y_2$ are the integration variables. The second iterated or the squared kernel $k^2_{\beta_j}(y_1, y_2)$ of our model is computed from (3.15) as

- for $y_1 \leq y_2$

$$\frac{-\beta_j^2\eta^3}{4}\left(\frac{e^{2i\beta_j y_2}}{\eta^3} + \frac{2e^{2i\beta_j}}{\eta^2} + \frac{2e^{-2i\beta_j(y_1-2)}}{\eta} + \frac{e^{-2i\beta_j(y_1-y_2-1)}}{\eta^2} + \frac{e^{-2i\beta_j(y_2-2)}}{\eta} + e^{-2i\beta_j(y_1+y_2-3)}\right),$$

- for $y_1 > y_2$

$$\frac{-\beta_j^2\eta^3}{4}\left(\frac{e^{2i\beta_j y_1}}{\eta^3} + \frac{2e^{2i\beta_j}}{\eta^2} + \frac{2e^{-2i\beta_j(y_2-2)}}{\eta} + \frac{e^{-2i\beta_j(y_2-y_1-1)}}{\eta^2} + \frac{e^{-2i\beta_j(y_1-2)}}{\eta} + e^{-2i\beta_j(y_1+y_2-3)}\right). \tag{3.45}$$

To approximate the solution $f$, Louis uses the following ansatz

$$f_\gamma(x) = \langle g, \psi^\gamma_x\rangle + \langle g, V^\gamma_x g\rangle, \tag{3.46}$$

where $x$ is the reconstruction point, $\psi^\gamma_x$ is the reconstruction kernel considered for the linearized operator $A_1$, and $V^\gamma_x$ is $M \times M$ matrix. If we replace $g$ by $\mathcal{A}f$ and use the properties of the inner product, we obtain

$$\begin{aligned} f_\gamma(x) &= \langle \mathcal{A}f, \psi^\gamma_x\rangle + \langle \mathcal{A}f, V^\gamma_x \mathcal{A}f\rangle \\ &= \langle A_1 f + A_2 f, \psi^\gamma_x\rangle + \langle A_1 f + A_2 f, V^\gamma_x (A_1 f + A_2 f)\rangle \qquad (3.47) \\ &\simeq \langle A_1 f, \psi^\gamma_x\rangle + \langle A_2 f, \psi^\gamma_x\rangle + \langle A_1 f, V^\gamma_x A_1 f\rangle. \end{aligned}$$

The $(\simeq)$ in the third line of equation (3.47) implies, that the high order terms are ignored as only a quadratic problem is considered. Thus, we have

$$f_\gamma(x) \simeq \langle A_1 f, \psi^\gamma_x\rangle + \langle A_2 f, \psi^\gamma_x\rangle + \langle A_1 f, V^\gamma_x A_1 f\rangle. \tag{3.48}$$

The linear term $\langle A_1 f, \psi_x^\gamma \rangle$ is approximated as for the case of linear operators. This means

$$\langle A_1 f, \psi_x^\gamma \rangle_Y \simeq \langle f, \delta_x^\gamma \rangle_X \,,$$

which coincides with (3.26)

$$A_1 A_1^* \psi_x^\gamma = A_1 \delta_x^\gamma.$$

The computation of the reconstruction kernel $\psi_x^\gamma$ follows as discussed in Section (3.3.1) for the linear case. If the linear term $\langle A_1 f, \psi_x^\gamma \rangle$ represents the solution, then the other two terms in equation (3.48) must be minimized as much as possible. As a result of this minimizing and since the kernels $\tilde{k}^1_{\beta_j}$ are linearly independent, then the matrix $V_x^\gamma$ is given by

$$V_x^\gamma = -\sum_{j=1}^{M} \psi_x^{\gamma,j} C_j.$$

Thus, from the ansatz (3.46), we obtain

$$f_\gamma(x) = \langle g, \psi_x^\gamma \rangle - \sum_{j=1}^{M} \psi_x^{\gamma,j} \langle g, C_j g \rangle \,, \tag{3.49}$$

where the matrices $C_j$ are independent of the reconstruction point $x$ and given by

$$C_j = (A_1 A_1^*)^{-1} B_j (A_1 A_1^*)^{-1}.$$

The matrices $B_j$ have the form

$$B_j = \int_0^1 \int_0^1 \tilde{k}^1(y_1) k^2_{\beta_j}(y_1, y_2) \tilde{k}^1(y_2)^T dy_1 dy_2, \quad \text{for each } j.$$

We denote with $\tilde{k}^1(y_2)^T$ the transpose of $\tilde{k}^1(y_2)$, and with $\tilde{k}^1(y_1), \tilde{k}^1(y_2)$ the vectors of $M$ components of $\tilde{k}^1_{\beta_j}(y_1), \tilde{k}^1_{\beta_j'}(y_2)$ respectively. We obtain

$$\begin{aligned} \tilde{k}^1(y_1) &= \frac{-\beta}{2i} \left( e^{2i\beta y_1} + \eta^2 e^{-2i\beta(y_1-2)} + 2\eta e^{2i\beta} \right), \\ \tilde{k}^1(y_2) &= \frac{-\beta'}{2i} \left( e^{2i\beta' y_2} + \eta^2 e^{-2i\beta'(y_2-2)} + 2\eta e^{2i\beta'} \right). \end{aligned} \tag{3.50}$$

For generalization to operators with arbitrary orders, we may refer to [43,60]. The numerical implementation of this method is treated in Chapter 4.

# Chapter 4

# Numerical Results

In this chapter, we apply the method of the Approximate Inverse for solving both the linearized and the quadratic inverse problems described in Chapter 3. In the case of the linearized problem, we compare our results with those obtained by applying the regularization method of Tikhonov-Phillips. Accomplishing accurate direct simulations is very helpful to test the proposed solution methods. These direct simulations check the equivalency between the BVP (2.19) and its integral formulation (2.27). Moreover, they generate the data for every given contrast function. This, in turn, assures us good test examples especially when dealing with space-dependent contrast functions. Depending on these data as an input, we solve the inverse problems which reconstruct the ARC's contrast function as an output.

## 4.1 Direct simulations

Recall the Lippmann-Schwinger integral equation (2.27):

$$u(x) + \int_0^1 \bar{k}_\beta(x,y)u(y)dy = u^0(x), \quad x \in (0,1), \tag{4.1}$$

where the kernel is given by:

$$\bar{k}_\beta(x,y) = \beta^2 k_\beta(x,y)f(y).$$

For computing a numerical integration using a quadrature rule we have

$$\int_\Omega \varphi(x)dx \approx \sum_{j=1}^{n} \omega_j \varphi(x_j),$$

where $\omega_j$ are the weights, $x_j$ are the discretization nodes of the interval $\Omega$ (in our model $\Omega = [0,1]$), and $n$ is the number of the discretization points.

We mainly apply Nyström method, see, *e.g.,* [15, 22, 33] to get the linear system

$$u(x) + \sum_{j=1}^{n} \omega_j \bar{k}_\beta(x, y_j) u(y_j) = u^0(x), \tag{4.2}$$

here $y_j = (j-1)h$ and the step-size $h_1 = 1/(n-1)$. We thus approximate the integral operator $K$ defined in (2.28) by a sequence of numerical integration operators

$$K_n u(x) = \sum_{j=1}^{n} \omega_j \bar{k}_\beta(x, y_j) u(y_j).$$

We also discretize the variable $x$ by setting $x_i = (i-1)h$ with $i = 1, ....., n$. Equation (4.2) becomes

$$u(x_i) + \sum_{j=1}^{n} \omega_j \bar{k}_\beta(x_i, y_j) u(y_j) = u^0(x_i). \tag{4.3}$$

The solution to the Fredholm integral equation of the second kind (4.1) is then approximated by solving the finite dimensional linear system (4.3).

For a fixed wave number $\beta$ and a given incident field $u^0(x)$ as in (2.24), we consider a contrast function $f(x)$ as an input embedded in $\bar{k}_\beta(x, y) = \beta^2 k_\beta(x, y) f(y)$ in (4.3). Then, we numerically compute the electric field $u(x)$ as an output. For the numerical computations, we use Matlab as a programming language, see, e.g., [26].

To test the accuracy of our system, we consider a test example for a homogeneous ARC. This means that we deal, as a first step, with the differential Helmholtz equation with constant coefficients. For such constant contrast functions, we compute the analytic electric field as a solution of the BVP (2.19) then we compare it with the numerical solution of the integral formulation (4.1).

**Test example 1** If we consider an arbitrary constant contrast function $f(x)$, then the BVP (2.19) becomes

$$(BVP) \begin{cases} u''(x) + c^2\beta^2 u(x) = & 0, \ x \in (0,1), \\ u'(0) + in_0\beta \ u(0) = & 2in_0\beta, \\ u'(1) - in_s\beta u(1) = & 0, \end{cases} \tag{4.4}$$

where the relation between the function $f$ and the constant $c$ is

$$c = \sqrt{1+f}.$$

The general solution of (4.4) is

$$u(x) = c_1 e^{+ic\beta x} + c_2 e^{-ic\beta x}, \tag{4.5}$$

where the constants $c_1$ and $c_2$ are computed to satisfy the boundary conditions in (4.4) as

$$c_1 = \frac{2(c+n_s)}{(1-c)(c-n_s)e^{2ic\beta} + (1+c)(c+n_s)}$$

$$c_2 = \frac{2(c^2-n_s^2)e^{2ic\beta}}{(1-c)(c^2-n_s^2)e^{2ic\beta} + (c+n_s)^2(1+c)}.$$

Alternatively, the general solution of (4.4) is given in terms of trigonometric functions as

$$u(x) = d_1 \cos(c\beta x) + d_2 \sin(c\beta x),$$

where the corresponding constants $d1$ and $d2$ are computed as

$$d_1 = \frac{2\beta\,[ci\cos(c\beta) + n_s \sin(c\beta)]}{\beta(c^2+n_s)\sin(c\beta) + ic\beta(1+n_s)\cos(c\beta)}$$

$$d_2 = \frac{i(2-d_1)}{c}.$$

A comparision between the exact field (4.5) as solution of equation (4.4) and the numerical field as solution of equation (4.3) is given in figures (4.1) and (4.2). The real and the image parts of the fields are considered in the both figures, respectively. In this example, the function $f(x) = 0.1$ is used as an input.

A similar comparison between the fields is given in figures (4.3) and (4.4). The function $f(x) = 0.52$ is used as an input in this example. Here we have chosen $\lambda = 4dn = 600.24$ where $d = 122\ nm$ and $n_{\text{ARC}} = 1.23$. This choice coincides with (A.16) and the discussion hereafter.

We test our direct simulation for many different constant contrasts. The related relative errors between the exact and the numerical fields are very small as soon as the wavelength is not smaller than 10 nanometres. These very small errors assure the equivalency between the BVP and its integral formulation in the sense of Theorem(2.2.1). Depending on these good results, we generate the data which will be used for solving the inverse problem. The Matlab-code prepared for this purpose is called *the direct solver*. For a given incident field, this code determines the total field for every input contrast function. As a result, we get the reflection coefficients which are the differences between the values of the incident and the total fields on the surface. The direct solver program is very important especially when dealing with space-dependent contrast function. This is because there is no explicit analytic formula for the related total field.

## 4.2 Inverse simulations

We test now the proposed reconstruction methods. We begin with the linearized inverse problem, check (3.13). We want to reconstruct the contrast function $f$ based on the given data or given reflection coefficients. This reconstruction is achievable by descretization, and then, reduction of the inverse problem into a system of linear equations. This system is not explicitly solvable for just one value $\beta$ of the wave numbers. In order to solve this system numerically, multiple values for the wave number $\beta$ have to be considered. According to [27, 40]; there is no unique solution to the inverse scattering problem, neither linearized nor normalized, for a single frequency.

This is also compatible with what we have in practice. The measurements correspond to a range of the wave lengths along the surface of the ARC. We take sampling of wave numbers $[\beta_{\min}, \beta_{\max}]$, we use the step-size $h_2 = (\beta_{\max} - \beta_{\min})/(M-1)$, where $M$ denotes the number of the wave lengths $\lambda_l, l = 1, ....., M$ taken in the interval $[\lambda_{\min}, \lambda_{\max}]$. The wave numbers at the boundaries are given by

$$\beta_1 = \beta_{\min} = \frac{2\pi d}{\lambda_{\max}} \quad \text{and} \quad \beta_M = \beta_{\max} = \frac{2\pi d}{\lambda_{\min}}. \tag{4.6}$$

The data is the difference between the values of the incident and the total fields at the surface of the ARC: $u(0,\beta) - u^0(0,\beta)$. For the case of reconstructing a constant contrast functions, we compute the data directly as we have the explicit formulas (2.24) and (4.5) of both incident and total fields, respectively. For the case of reconstructing a space-dependent contrast functions, we introduce the following example.

**Test example 2** We rewrite the BVP (2.19) in terms of the Helmholtz differential equation with a variable refractive index, we obtain

$$(BVP) \begin{cases} u''(x) + \beta^2 n^2(x) u(x) = & 0, \ x \in (0,1), \\ u'(0) + in_0\beta \ u(0) = & 2in_0\beta, \\ u'(1) - in_s\beta u(1) = & 0, \end{cases} \tag{4.7}$$

with $n^2 = 1 + f$. The formula which connects the space-dependent refractive index $n$ with the field $u$ is given by:

$$u(x) = \frac{1}{\sqrt{\beta n(x)}} \left( A(x) e^{iS(x)} + B(x) e^{-iS(x)} \right), \tag{4.8}$$

$$u'(x) = i\sqrt{\beta n(x)} \left( A(x) e^{iS(x)} - B(x) e^{-iS(x)} \right), \tag{4.9}$$

where

$$S(x) = \beta \int_0^x n(\zeta) d\zeta.$$

The first derivatives of the functions $A(x)$ and $B(x)$ are

$$A'(x) = \frac{n'(x)}{2n(x)} B(x) e^{-2iS(x)} \quad \text{and} \quad B'(x) = \frac{n'(x)}{2n(x)} A(x) e^{2iS(x)}.$$

We choose the contrast function $f(x)$, which we want to reconstruct, to be the function

$$f(x) = \begin{cases} x & \text{for} \quad 0 \leq x \leq \frac{1}{2} \\ \\ 1 - x & \text{for} \quad \frac{1}{2} < x \leq 1 \end{cases} \tag{4.10}$$

After some calculations we obtain

$$S(x) = \begin{cases} \frac{2\beta}{3} \left[ (x+1)^{3/2} - 1 \right] & \text{for} \quad 0 \leq x \leq \frac{1}{2} \\ \\ \frac{2\beta}{3} \left[ 2.6742 - (2-x)^{3/2} \right] & \text{for} \quad \frac{1}{2} < x \leq 1. \end{cases}$$

An analytic computation of the field $u$ (4.8), requires finding explicit formulas of the functions $A(x)$ and $B(x)$. This is mostly replaced by numerical computations, we refer to [7, 41, 57] for more details. Thus, it is also advantageous making use of our direct solver, which numerically computes the field and then generate the required data for solving the inverse problem.

We consider the interval of the wave numbers $[\beta_{\min}, \beta_{\max}]$. We seek the value of the total field at the point $x = 0$. The direct solver computes $M-$times the difference $u(0, \beta) - u^0(0, \beta)$. This, in turn, generates our data, check (3.10).

To ensure the validity of the Born approximation, the contrast function $f(x)$ and the interval $[\beta_{\min}, \beta_{\max}]$ must satisfy the condition

$$\beta \sup_{x \in (0,1)} |f(x)| < 4\pi b, \tag{4.11}$$

where $b$ is a small constant, e.g., $b = 0.16$ or $b = 0.2$.

The relative errors in the linear and quadratic approximations for the reconstructed function $f(x)$ are defined respectively as

$$\delta_{\text{lin}} := \frac{\| f_{\text{lin}} - f_{\text{exact}} \|_{L_2(0,1)}}{\| f_{\text{exact}} \|_{L_2(0,1)}}$$

$$\delta_{\text{quad}} := \frac{\| f_{\text{quad}} - f_{\text{exact}} \|_{L_2(0,1)}}{\| f_{\text{exact}} \|_{L_2(0,1)}}$$

where $f_{\text{lin}}$ and $f_{\text{quad}}$ denote the contrast functions computed using the linear and the quadratic approximations respectively.

Firstly, we deal with the linear approximation. For the inversion, the reconstruction kernel $\psi_x^\gamma$ is computed numerically as a solution of equation (3.35) independently of the data. In this computation, we use the Gaussian mollifier described in equation (3.24). Next, we compare the calculated results of the Tikhonov-Phillips method to those of the method of the Approximate Inverse. For the reconstruction procedure, the equations (3.23) and (3.28) are applied to the two methods respectively.

Beginning with **test example 1**, we applied the method of AI to reconstruct the constant contrast function $f(x) = 0.1$. The reconstruction was achieved in the interval $[40, 900]$. See Figure (4.5). As previously mentioned, satisfying the validity of the Born Approximation is crucial for the successful application of the reconstruction methods. Attempting to reconstruct the same function in the interval $[15, 900]$ results with bad reconstruction. This is because of not respecting the aforementioned validity condition, see Figure (4.6). For the reconstruction of the space-dependent contrast function $f = \frac{1}{4}y$, see Figure (4.7). The data here are generated using the direct solver.

In the case of **test example 2**, the validity of the first iteration of the Born approximation is checked in the interval $[\beta_{\min}, \beta_{\max}]$. For that purpose, we established a comparison between the numerical solutions of two equations. These are equation (4.1) and the one-time linearized integral equation (3.10). The result is shown in Figure (4.8). Figure (4.9) shows the outcomes of applying both methods; TP and AI to reconstruct the function in this example. A reconstruction of the same function, with perturbed data, is presented in Figure (4.10).

Secondly, we discuss the case of the quadratic approximation. For that purpose, the validities of both, the first and the second iterations of the Born approximation are checked in the interval $[\beta_{\min}, \beta_{\max}]$. In this case, an additional comparison is needed. This is due to having a third equation attributed to second iteration of the Born approximation. This equation is the two-time linearized integral equation (3.8). The two remaining equations to be compared are (4.1) and (3.10). See Figure (4.11). Figures (4.12) and(4.13) show the outcomes of applying the method of AI to both, linear and quadratic approximations to reconstruct the function in test example 2. A reconstruction with perturbed data is presented in Figure (4.14).

## 4.3 Adaptive modeling

An efficient alternative way to improve the linear approximation is to use a threshold to decide where to apply a higher (quadratic) order of approximation. This leads to what we call adaptive modeling. We take here advantage of the method of the Approximate Inverse which is a local method. Hence, we seek some criterion which evaluates the quality of the linear reconstruc-

tion in every part of the function $f$. Such a criterion depends on the validity of the Born approximation. For fixed frequency, the Born condition depends on the strength of the contrast $f$. By setting another upper-bound for the contrast as a threshold, we can locally choose where we need to apply the quadratic approximation. In Figure (4.9), it is clear that the parts of the function that match low contrasts are well-reconstructed. This is due to matching the Born approximation which is valid for low contrasts. We recall the global validity-condition (4.11)

$$\beta \sup_{x\in(0,1)} |f(x)| < 4\pi b, \tag{4.12}$$

with $b = 0.2$. The aforementioned criterion assumes a stronger condition than (4.12), namely the computable condition with the linear approximation $f_{\text{lin}}$ of $f$

$$\beta \sup_{x\in(0,1)} |f_{\text{lin}}(x)| < \pi b. \tag{4.13}$$

The low contrasts and respectively the parts of the function which obey the *a-posteriori* condition (4.13), are well reconstructed by the linear approximation. For these parts, there is no need to accomplish any approximation of higher order. Numerically, we prepare a small Matlab-code to implement this criterion. The resulting vector, has a length $N$, where $N$ represents the number of the discretization points chosen in the reconstruction interval $(0, 1)$. The nonzero values in this vector coincide with the good reconstructed parts in the function. However, the zero values leads to the parts, which need higher order of reconstruction. The quadratic approximation is used then only to improve the reconstruction in these relevant parts, which are not good reconstructed. Comparing equations (3.49) and (3.28), we see that the corrections $C$ achieved in the quadratic approximation are given by

$$C(x) = -\sum_{j=1}^{M} \psi_x^{\gamma,j} \langle g, C_j g\rangle . \tag{4.14}$$

These corrections were computed numerically for each sampling of the generated data. During this numerical computation, the method of Tikhonov-Phillips was used to find the inverse of the ill-conditioned Gram matrix (3.39). Thus, we consider the corrections described in equation (4.14) for the improvement of the reconstruction only in the relevant parts. Figure (4.15) stands for the comparison between both, the linear and the quadratic approximations using the idea of the adaptive modeling. See also Figure (4.16) for the reconstruction of the Ramp function.

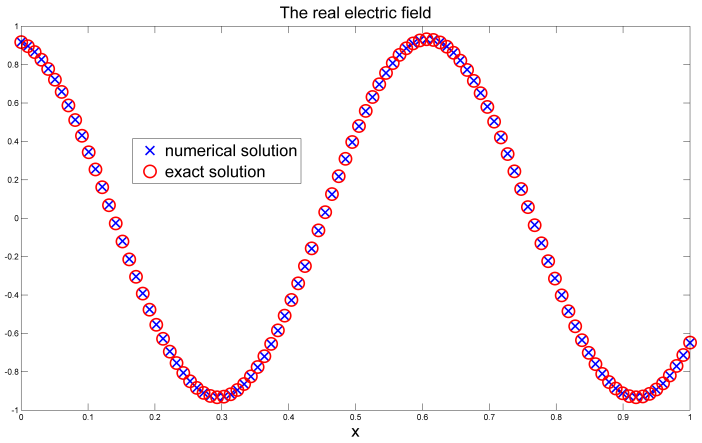


**Figure 4.1:** Direct Simulation: $L_2 -$ Relative error $= 0.0023$ with fixed wave length $\lambda = 80\ nm$, for reconstruction of the of the field in its real part.

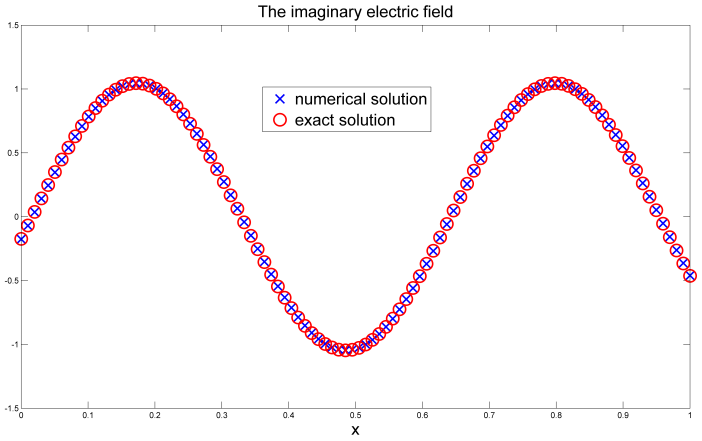


**Figure 4.2:** Direct Simulation: The image part of the field considered in the Figure above

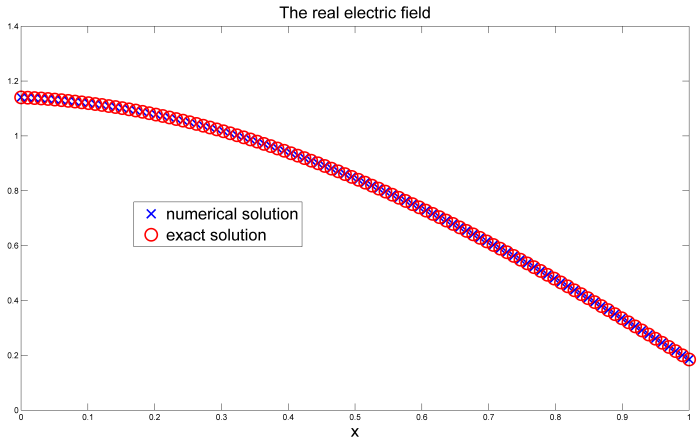


**Figure 4.3:** Direct Simulation: $L_2 -$ Relative error $= 0.0016$ with fixed wave length $\lambda = 600.24\ nm$, for the reconstruction of the of the field in its real part.

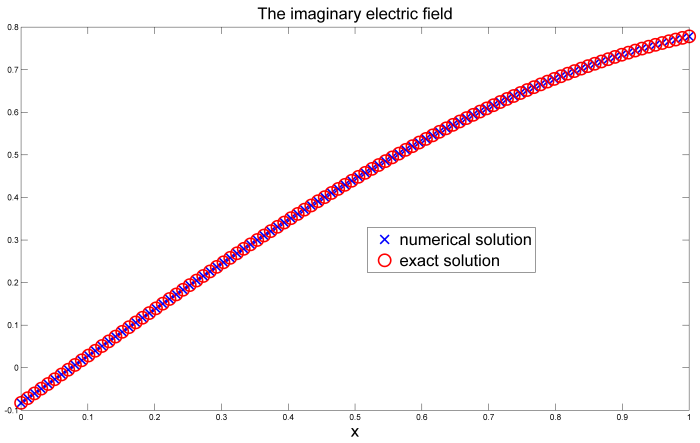


**Figure 4.4:** Direct Simulation: The image part of the field considered in the Figure above.

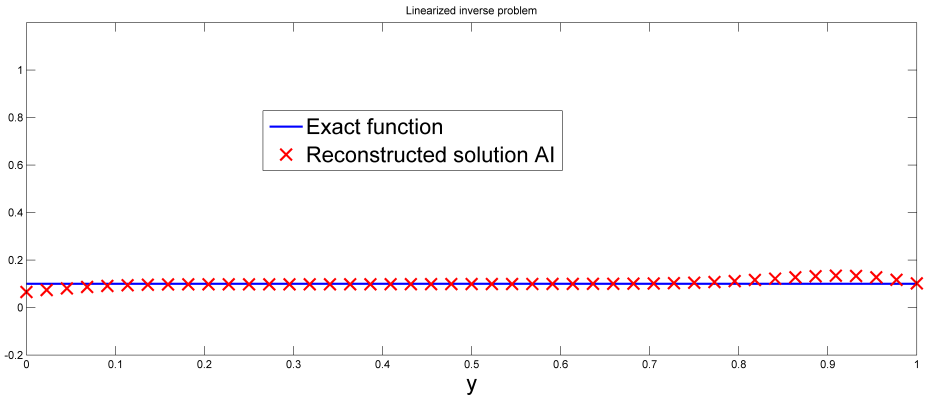


**Figure 4.5:** The inverse problem: Reconstruction of $f(x) = 0.1$ in the wavelength interval $[40, 900]$ $nm$, $\delta_{\text{lin}} = 0.1350$ for the method of AI.

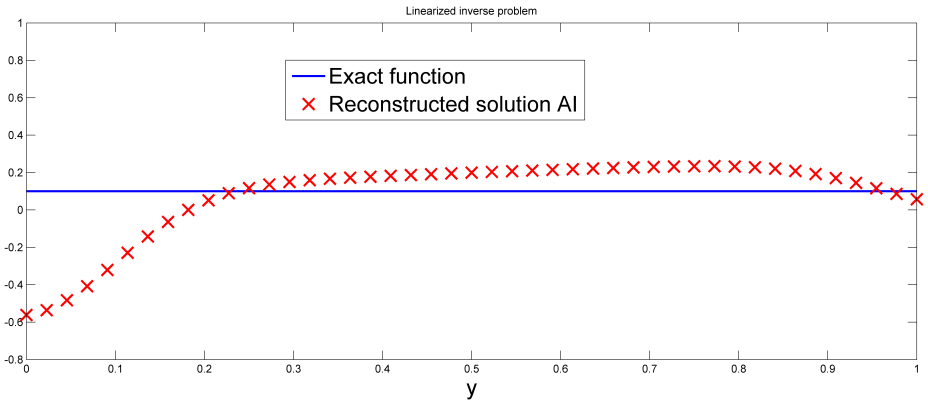


**Figure 4.6:** Inverse simulation: Bad reconstruction of $f(x) = 0.1$ in the wavelength interval $[15, 900]$ $nm$. Since this interval does not satisfy the validity of Born approximation (4.11). $\delta_{\text{lin}} = 2.0911$ for the method of AI

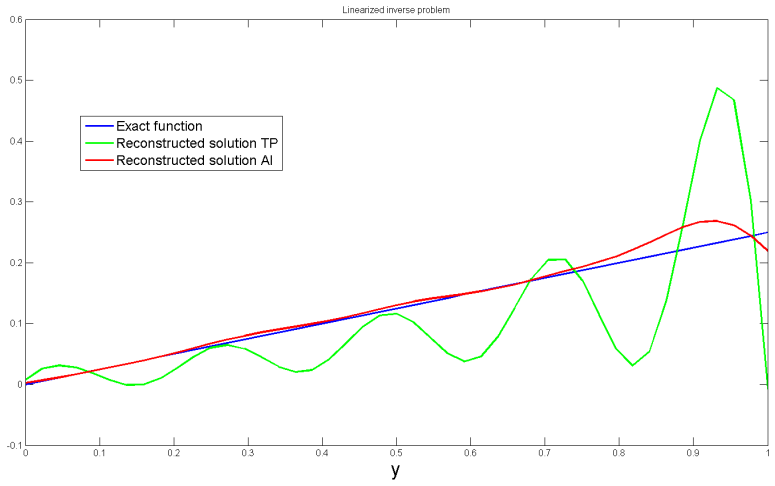


**Figure 4.7:** The inverse problem: Reconstruction of the function $f = \frac{1}{4}y$ for exact solution (in blue) and reconstructed solution for the AI (in red) and TP (in green) as methods of regularization. The relative errors are $\delta_{\text{lin}} = 0.0904$ and 0.6139, respectively, with simulated data considered for a wave lengths ranging between 60 and 1300 $nm$.

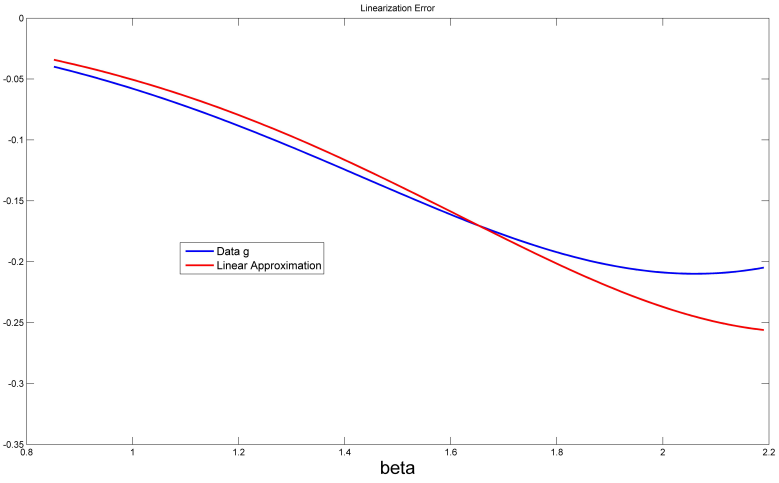


**Figure 4.8:** Linearization validity: $L_2-$Relative error $= 0.1178$ for simulated data (in blue) and one-time linearized data (in red) using the first Born approximation where Example (4.10) is considered for a wave lengths ranging between 350 and 900 $nm$.

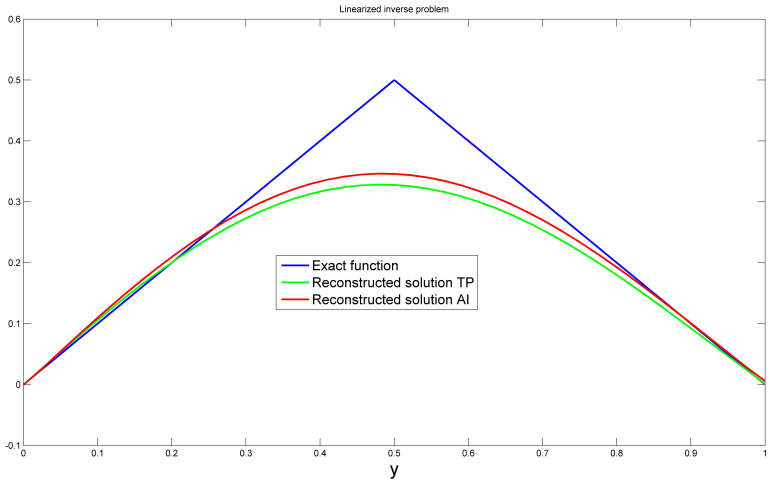


**Figure 4.9:** The inverse problem: Reconstruction of Example (4.10) for exact solution (in blue) and reconstructed solution for the Approximate Inverse (in red) and Tikhonov-Phillips (in green) as methods of regularization. The relative errors are $\delta_{\text{lin}} = 0.1911$ and $0.2282$ respectively, with simulated data considered for a wave lengths ranging between 350 and 900 $nm$.

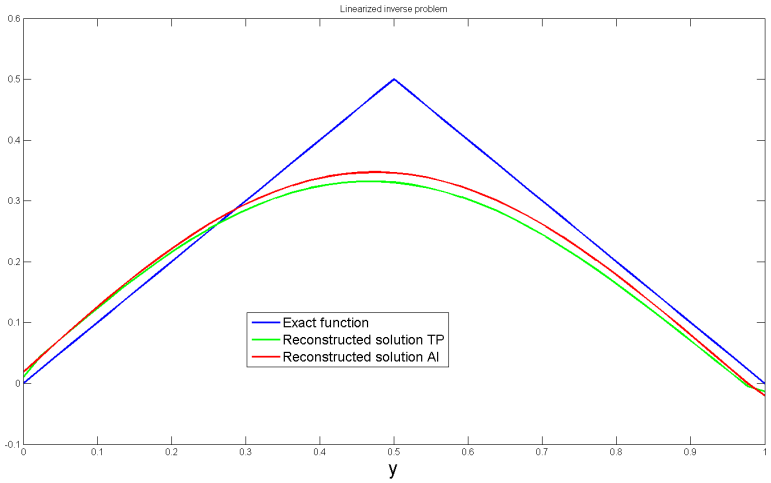


**Figure 4.10:** The inverse problem: Reconstruction of Example (4.10) with perturbed data of level 0.2% with relative errors $\delta_{\text{lin}} = 0.1996$ and $0.2336$ for AI and TP respectively

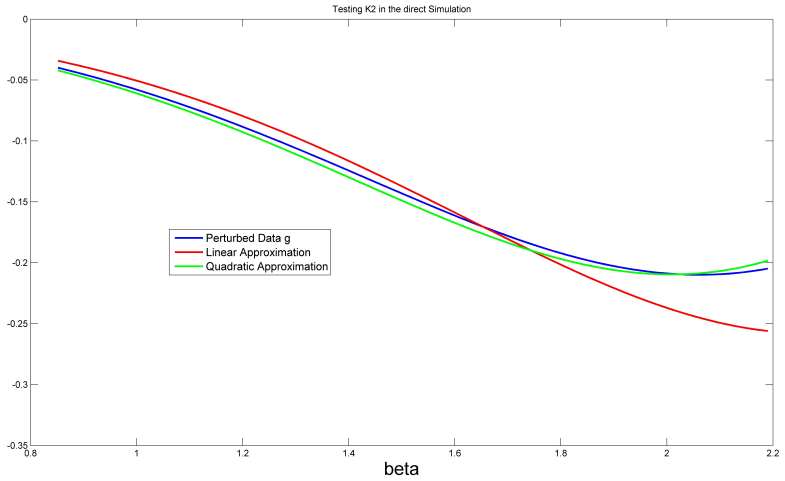


**Figure 4.11:** Linearization validity of both first and second iterations of Born: $L_2$ – Relative errors are 0.1178 and 0.0291 respectively. For simulated data (in blue), one-time linearized data (in red), and two-times linearized data (in green)

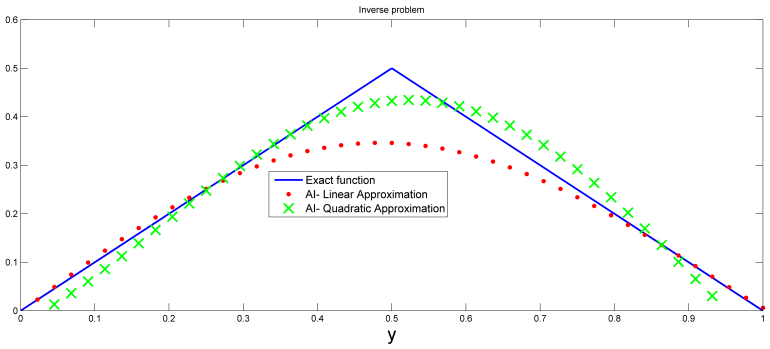


**Figure 4.12:** The inverse problem: Reconstruction of Example (4.10) for exact solution (in blue), reconstructed solution for AI- linear approximation (in red), and for AI- quadratic approximation (in green). The relative errors are $\delta_{\text{lin}} = 0.1911$ and $\delta_{\text{quad}} = 0.1079$ respectively, with simulated data considered for a wave length ranging between 350 and 900 $nm$.

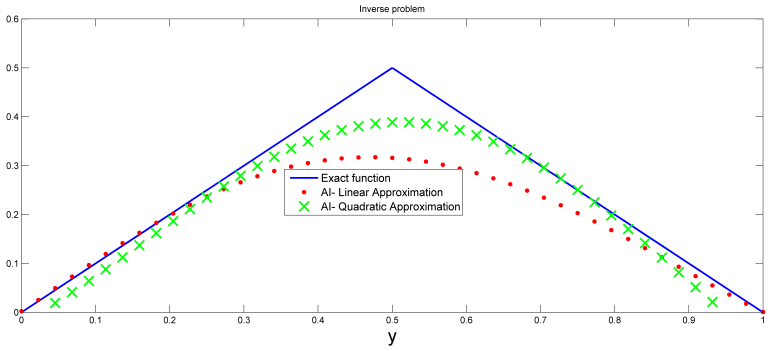


**Figure 4.13:** The inverse problem: Another reconstruction of Example (4.10) for exact solution (in blue), reconstructed solution for AI- linear approximation (in red), and for AI- quadratic approximation (in green).

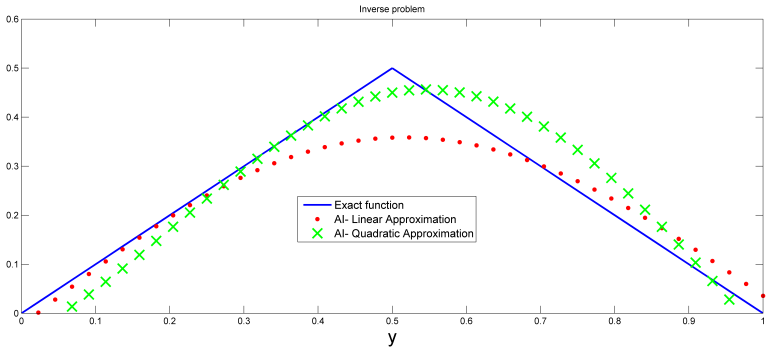


**Figure 4.14:** The inverse problem: Reconstruction of Example (4.10) with perturbed data of level 0.15 %.

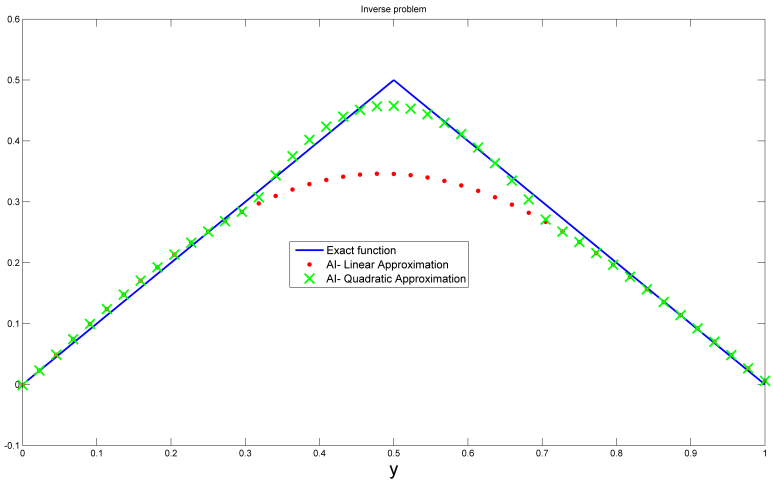


**Figure 4.15:** The inverse problem ( Adaptive modeling): Reconstruction of Example (4.10) for exact solution (in blue), reconstructed solution for AI- linear approximation (in red), and for AI- quadratic approximation (in green). The corrections are partially considered. The relative errors are $\delta_{\text{lin}} = 0.1911$ and $\delta_{\text{quad}} = 0.0418$ respectively.

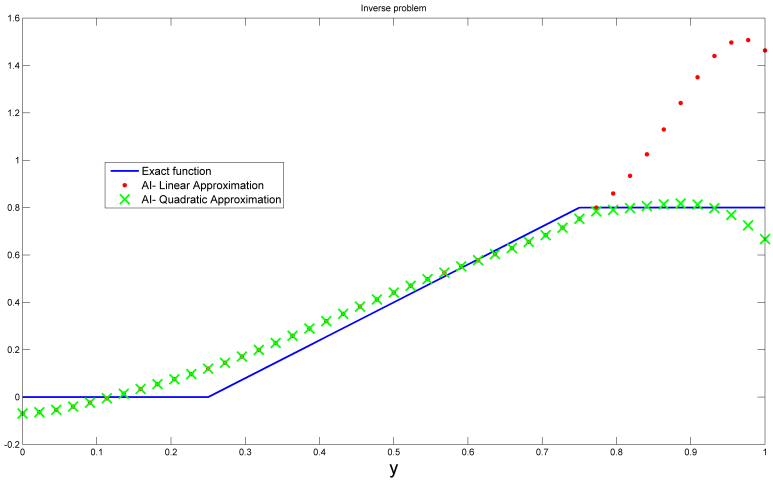


**Figure 4.16:** The inverse problem ( Adaptive modeling): Reconstruction of the Ramp function for exact solution (in blue), reconstructed solution for AI- linear approximation (in red), and for AI- quadratic approximation (in green). The corrections are partially considered.

### Short discussion

We first solved the direct problem accurately as shown in Figures (4.1) through (4.4). This was done by applying the Nyström quadrature method to solve Fredholm integral equation. Based on that, we prepared a direct solver to generate the data, which are required to solve the inverse problem. Secondly, we checked the validity of the Born approximation. Any interval that does not satisfy the validity of the Born approximation leads to a bad reconstruction as shown in Figure (4.6). The reconstruction of the space-dependent contrast function $f = \frac{1}{4}y$ in Figure (4.7) assures that the Born approximation is valid for low contrasts. The lower the contrast the better the reconstruction. This validity was also checked for the case of test example 2 in Figure (4.8). The next step was to test the stability of the method of the Approximate Inverse in comparison to the method of Tikhonov-Phillips. We then checked the validity of the second iteration of the Born approximation as in Figure (4.11). Figures (4.12) and (4.13) showed the improvement achieved by applying the quadratic approximation. The nonlinear part was responsible for the middle error in the result. Although there was no data error in the middle, see Figure (4.15). The choice of the regularization parameters in both, the linear and the quadratic approximations was achieved empirically. The approach was fast, since during the computation of the nonlinear coefficients, the same Gram matrix was reused. This, in turn, reduced the computation time.

# Conclusion

In this research, we solved an inverse scattering problem for the design of Anti-Reflection Coatings. The main objective in the inverse problem was to determine the space-dependent refractive index of some coating from prescribed reflection coefficients on the surface. The more general case of an inhomogeneous ARC was discussed. For modeling the light propagation through a stratified isotropic medium, we reduced the time-harmonic Maxwell's equations into a one-dimensional Helmholtz equation with prescribed boundary conditions. From the resulting boundary value problem, we derived an equivalent formulation as a Fredholm integral equation of the first kind. The difficulty in inverse scattering problems is twofold as they are nonlinear and ill-posed. We applied an iterated Born approximation for linearizing the relevant nonlinear mathematical model. The second iteration of the Born approximation was used to approximate the nonlinear problem. We solved both the linearized and the quadratic problems using the efficient method of the Approximate Inverse. We developed a direct solver based on Nyström quadrature method for solving the integral equation of the second kind. Using the direct solver, it was possible to generate the data for a known contrast function. We checked the validity of the Born approximation as a linearization method of the nonlinear inverse problem. We tested the stability of the method of the Approximate Inverse in comparison to the widely used Tikhonov-Phillips regularization method. Observing the outcomes of the numerical simulations provided evidence for the better performance achievable by the method of the Approximate Inverse. The method was extended by Louis using nonlinear approximation of higher order. This extension enabled applying the method to solve the nonlinear inverse problem using the quadratic approximation. The validity of the second iteration of the Born approximation is checked. It was shown that the quadratic approximation did, in fact, improve the linear approximation considerably.

# Outlook

As interesting issues for further investigations we can mention:

- The validation of the numerical method presented in this contribution by using experimentally-generated data.

- Computing the singular value decomposition of the relevant linearized operator. This is important, not only to apply and compare an additional classical regularization method, but also to find another way for the computation of the inverse Gram matrix. Such a matter may be helpful for solving the quadratic problem.

- The applicability of the approach in the optimal design of some higher dimensional models and thin-film structures. For example, diffraction gratings, guided-mode grating resonant structures, as well as models with omnidirectional Anti-Reflection properties.

- A complete discussion about the diversity of the wave numbers required for solving the inverse problem.

- Finding an optimal implicit criterion to be used in the adaptive modeling.

# Appendices

# Appendix A

# Physical Background

In this Appendix we discuss some elementary physical concepts related to our model. We start with the importance of solar energy in comparison to other energy resources. Then we talk about the solar photovoltaics, history, types and the efficiency of the solar cells. Next, we describe the concept of Anti-Reflection Coatings (ARCs) to see how they improve the efficiency of the solar cells. We deduce the coefficients of light transmission and reflection and compare them for some different interfaces.

## Solar energy and other energy resources

**Solar energy** represents largest and most important renewable energy resource. Examples for other energy renewable resources are hydroelectric power, wind power, bioenergy, shallow geothermal energy, and deep geothermal energy. The natural resources of nuclear materials and fossil fuel are limited. Therefore, their production will be expensive in the future. The cost of crude oil prospecting increases and so does the cost of the energy used to generate it hereafter.

The constant that represents the average power density of the solar radiation outside the the Earth atmosphere is called **the solar constant**. It is specified according to well-established measurements and equals 1366 W/ $m^2$. The total annual solar energy which arrives to the surface of Earth is $5.46 \times 10^{24}$ J. The J denotes the **Joule** the energy measurement unit. Although there exists a 30% reflected loss of the solar radiation reaching the Earth, in addition to a 20% absorbed loss into the sky clouds, nearly 0.01% of the aforementioned annual solar energy can cover the energy demand of the entire world. The following equation evaluates the worth of an energy production [10]:

$$\text{Energy Balance or EROI} = \frac{\text{energy return}}{\text{investment}} = \frac{\text{energy in a volume of fuel}}{\text{energy required to produce it}},$$

with EROI standing for energy return on investment. For example, the value of energy balance in the crude oil production was about 100 in the 1930s, while it dropped to 25 in 1970s. The solar electricity is based on a well established technology that is constantly being improved by scientists in the field. Therefore, the value of their energy balance is expected to grow up in the coming years. With this steady increase in the value of the solar electricity, one can prospect their prevalence as an alternative of the classical energy productions. For more information we may refer to *e.g.* German Solar Industry Association[1].

## Solar photovoltaics and solar cells

A well-established predicts report that the worldwide energy demand can't be supported by only depending on the fossil fuel. One of the solar energy applications is the solar water heaters. These heaters can cover just a decent part of the whole energy demand. **Solar photovoltaics** come as a suitable replacement of the old fossil energy. Solar photovoltaic energy is not only the most, but also the fastest increasing energy technology to date.
**Photovoltaics (PV)** is a method for generating electric power using the solar cells by converting the sun light, as a flow of photons, into electricity. **Solar cells** are solid-state devices used in the above mentioned technology to convert the solar radiations into a flow of electrons.

**Figure A.1:** Crystalline silicon solar cells in the Nellis Solar Cell Planet, located within Nellis Air Force Base in Nevada- US. Photo source is [10]

[1] www.solarwirtschaft.de

**Efficiency of solar cells**

According to American Society for Testing and Materials: In order to evaluate their efficiency, solar cells must satisfy standard illumination conditions, these are:

- intensity of 1000 W/ $m^2$,
- ambient temperature of 25°C,
- a sunlight spectrum passed through the atmosphere into the cells, when the elevation between the sun and the horizon is at 42°.

Respecting the above mentioned illumination conditions in addition to reaching the maximun power point [10], the efficiency of solar cells is defined with the following ratio

$$\textbf{Efficiency} = \frac{\text{Output power as electricity}}{\text{Input power as solar radiation}}.$$

**Solar cells, types and history**

In the 1870s, when the first solar cells were made, selenium was the material of choice. However its poor efficiency (about 0.5%) motivated research for better materials for this purpose. More efficient discovered materials are the modern crystalline silicon solar cells designed and demonstrated in 1954s by Gerald Pearson, Darryl Chapin and Calvin Fuller. The related research project was first established in 1953s in Bell Laboratories in Berkeley Heights, New Jersey, US. The efficiency of the silicon solar cells started from 5.7% at that time, which is ten time more than that obtained from selenium, and has been improved to 24% before 2000s. These crystalline silicon solar cells occupy the largest proportion of the market share with about 80%. They vary in two main types: monocrystalline and polycrystalline silicon solar cells, see Table (A.1)

| Type | Efficiency (%) | Cost $/Wp | Market share (%) |
|---|---|---|---|
| Monocrystalline Si | 17-20 | 3.0 | 30 |
| Polycrystalline Si | 15-18 | 2.0 | 40 |
| Amouphous Si | 5-10 | 1.0 | 5 |
| CIGS | 11-13 | 1.5 | 5 |

**Table A.1:** Comparision between some types of solar cells, table source is [10]

where Wp denotes the peak watt which is the power (in watts) produced by solar module under standard illumination conditions. Other types of solar

cells are the thin-film solar cells, like the amorphous silicon solar cells which is less-efficient than the first two types. Other examples of thin-film solar cells are those made from CIGS (copper, indium, gallium, selenide) and CdTe-CdS, they lie after the crystalline silicon ones in market share. The newest but not yet high efficient are the organic solar cells. The policy in the economy and the improvement in the Photovoltaics technology had a key role in decreasing the price of solar cells. It is worth mentioning some factors behind the general price-differences in the various types of solar cells. Such factors include: efficiency, life time, and the amount of materials needed for manufacturing ,e.g., silicon feedstock, wafers and ingot and the production itself.

## Anti-Reflection Coatings

**Anti-Reflection Coatings (ARCs)** are thin films deposited, e.g., onto solar cells to enhance their efficiency by reducing the reflected light, see Figure (A.2).

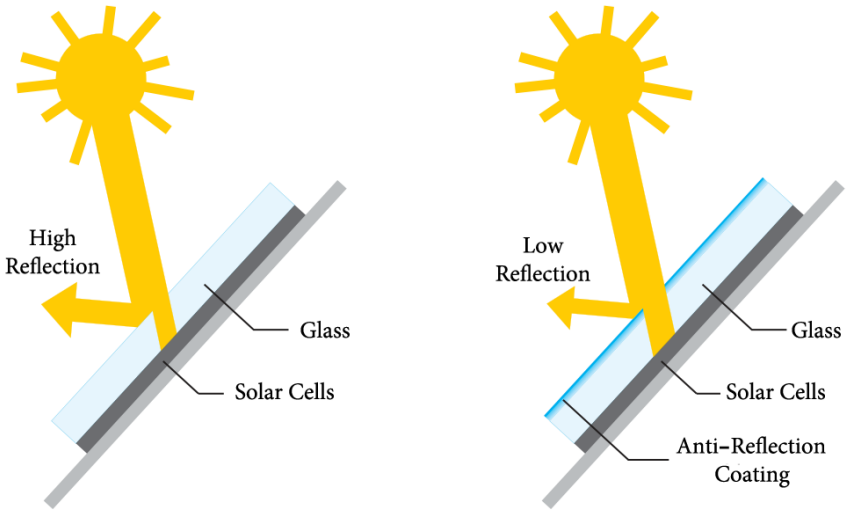


**Figure A.2:** The setting of the ARC onto solar cells.

Anti-Reflection Coatings were invented in early twentieth century, and since then they have found several fields of applications, e.g., camera lenses, ophthalmics, displays, optical-fiber devices and microscopes.
The **Refractive index** of some medium is defined as

$$n \equiv \frac{c}{v},$$

where $c$ is the speed of light in a vaccum and $v$ is the speed of light in this medium.

**Coefficients of transmission and reflection**

Assume that we have some classical silicon solar cell without ARCs. We want to evaluate the transmission and reflection of the light at normal incidence (incident angle $\theta = 0$) on the interface of this silicon solar cell at $x = 0$, see Figure (A.3). We follow [10] and consider two media, the first medium is the air environment with refractive index $n_0 = 1$ and the second medium is a silicon solar cell with refractive index $n_{\text{si}} = 3.49$. The incident wave $e^{i\kappa n_0 x}$ with the $x$-axis as a direction of propagation has the free space wavenumber $\kappa$ as

$$\kappa = \frac{wn_0}{c},$$

where the frequency is denoted by $\omega$ and $c$ stands for the speed of the light in the vacuum. The electric and magnetic fields intensities $\mathcal{E}$ and $\mathcal{H}$ of the incident wave are computed via the following formulas:

$$\mathcal{E}_{\mathcal{I}} = \mathcal{I}e^{i(\kappa x - \omega t)}, \tag{A.1}$$

$$\mathcal{H}_{\mathcal{I}} = \frac{n_0}{c}\mathcal{I}e^{i(\kappa x - \omega t)}, \tag{A.2}$$

respectively, where $\mathcal{I}$ is a constant which denotes the incident light intensity.

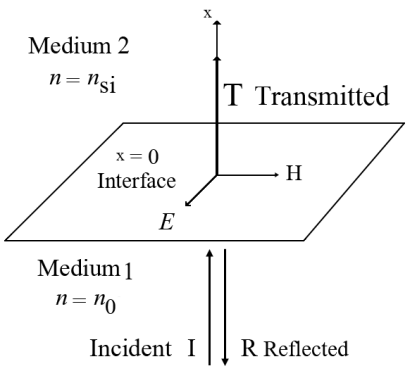


**Figure A.3:** Medium 1 is a vacuum and medium 2 is a silicon solar cell without ARC.

The wavenumber for the light transmitted into the silicon medium is given by

$$\kappa_{\mathcal{T}} = \frac{wn_{si}}{c}.$$

The electric and magnetic fields intensities of the transmitted wave are

$$\mathcal{E}_{\mathcal{T}} = \mathcal{T}e^{i(\kappa_{\mathcal{T}} x - \omega t)},$$

$$\mathcal{H}_{\mathcal{T}} = \frac{n_{\text{si}}}{c}\mathcal{T}e^{i(\kappa_{\mathcal{T}}x-\omega t)},$$

respectively, where $\mathcal{T}$ is a constant which denotes the intensity of the transmitted light. The reflected wave lies in the same medium as the incident wave (air environment). Both of them have the same absolute value, however, their directions are reversed with respect to the $x$-axis. Thus the electric and magnetic fields intensities of the reflected wave are given by

$$\mathcal{E}_{\mathcal{R}} = \mathcal{R}e^{i(-\kappa x-\omega t)},$$

$$\mathcal{H}_{\mathcal{R}} = \frac{-n_0}{c}\mathcal{R}e^{i(-\kappa x-\omega t)}, \tag{A.3}$$

with $\mathcal{R}$ a constant which denotes the intensity of the reflected light.

The electric and magnetic fields intensities are continuous at the interface $x = 0$, which implies that:

$$\mathcal{E}_{\mathcal{I}} + \mathcal{E}_{\mathcal{R}} = \mathcal{E}_{\mathcal{T}}, \tag{A.4}$$

$$\mathcal{H}_{\mathcal{I}} + \mathcal{H}_{\mathcal{R}} = \mathcal{H}_{\mathcal{T}}. \tag{A.5}$$

We substitute equations (A.1)-(A.3) in (A.4),(A.5) to get:

$$\mathcal{I} + \mathcal{R} = \mathcal{T}, \tag{A.6}$$

$$n_0(\mathcal{I} - \mathcal{R}) = n_{\text{si}}\mathcal{T}. \tag{A.7}$$

Solving equations (A.6), (A.7) is straightforward and leads to the following formulas, known as **Frensel formulas**:

$$\mathcal{R} = \frac{n_0 - n_{\text{si}}}{n_0 + n_{\text{si}}}\mathcal{I}, \tag{A.8}$$

$$\mathcal{T} = \frac{-2n_{\text{si}}}{n_0 + n_{\text{si}}}\mathcal{I}. \tag{A.9}$$

The power density of the electromagnetic field or the Poynting vector is defined as in [10, Chapter 2]:

$$\mathcal{S} = \frac{1}{\mu_0}\mathcal{E} \times \mathcal{H},$$

where $\mu_0$ denotes the permeability of the free space. Now, we compute the magnitudes of the power densities of the incident, transmitted, and reflected

light respectively:

$$\mathcal{S}_{\mathcal{I}} = \frac{1}{\mu_0}\mathcal{E}_{\mathcal{I}} \times \mathcal{H}_{\mathcal{I}} = \frac{n_0}{\mu_0 c}\mathcal{I}^2 e^{-2i\omega t},$$

$$\mathcal{S}_{\mathcal{T}} = \frac{1}{\mu_0}\mathcal{E}_{\mathcal{T}} \times \mathcal{H}_{\mathcal{T}} = \frac{n_{\mathrm{si}}}{\mu_0 c}\mathcal{T}^2 e^{-2i\omega t},$$

$$\mathcal{S}_{\mathcal{R}} = \frac{1}{\mu_0}\mathcal{E}_{\mathcal{R}} \times \mathcal{H}_{\mathcal{R}} = \frac{-n_0}{\mu_0 c}\mathcal{R}^2 e^{-2i\omega t}.$$

The nondimensionalised **transmission and reflection coefficients** are defined respectively as:

$$\mathcal{T} \equiv \frac{\mathcal{S}_{\mathcal{T}}}{\mathcal{S}_{\mathcal{I}}} = \frac{4n_0 n_{\mathrm{si}}}{(n_0 + n_{\mathrm{si}})^2}, \tag{A.10}$$

$$\mathcal{R} \equiv \frac{\mathcal{S}_{\mathcal{R}}}{\mathcal{S}_{\mathcal{I}}} = -\left(\frac{n_0 - n_{\mathrm{si}}}{n_0 + n_{\mathrm{si}}}\right)^2. \tag{A.11}$$

**Example** we compute now the percentages of the transmission and reflection coefficients in the aforementioned setting:

$$\mathcal{T}_{\mathrm{si}} \equiv 400 \times \frac{3.49}{(1+3.49)^2}\% \approx 69.24\% \tag{A.12}$$

$$\mathcal{R}_{\mathrm{si}} \equiv -100 \times \frac{(1-3.49)^2}{(1+3.49)^2}\% \approx 30.76\% \tag{A.13}$$

Thus there is about 30% loss of sunlight in that classical case.

**The importance of ARCs**

To minimize the light-loss we consider now the last example after depositing a glass substrate above the solar cell. From equations (A.10), (A.11) we compute the percentages of the transmission and reflection coefficients in this new setting. The refractive indices of a vaccum and a glas are $n_0 = 1$ and $n_{\mathrm{Glass}} = n_s = 1.52$ respectively, we find:

$$\mathcal{T}_{\mathrm{s}} \equiv 400 \times \frac{1.52}{(1+1.52)^2}\% \approx 95.75\%,$$

$$\mathcal{R}_{\mathrm{s}} \equiv -100 \times \frac{(1-1.52)^2}{(1+1.52)^2}\% \approx 4.25\%.$$

The less the refractive index of the upper medium, the less the reflected sunlight and the more the absorbed sunlight.

One more practical step is to install another layer with a lower refractive index above the glass one. The idea is to approximately eliminate or reduce the reflected light. The role of ARCs here is to try to satisfy the desired full light absorption. They have low refractive indices, varying in the interval $(n_{\text{Vaccum}}, n_{\text{Glass}})$. We compute now the percentages of the transmission and reflection coefficients at the surface $x = 0$ in the newest setting. We consider some ARC with thickness $d$ equals to the quarter wavelength in this coating $\lambda = 4dn_{\text{ARC}}$. This coating has the refractive index $n_{\text{ARC}} = 1.23$, we obtain

$$\mathcal{T}_{\text{ARC}} \equiv 400 \times \frac{1.23}{(1+1.23)^2}\% \approx 98.93\%, \tag{A.14}$$

$$\mathcal{R}_{\text{ARC}} \equiv -100 \times \frac{(1-1.23)^2}{(1+1.23)^2}\% \approx 1.06\%. \tag{A.15}$$

Thus, the new setting is necessary to reduce the loss in the incident light to about 30%. The reason of choosing $n_{\text{ARC}} = 1.23$ is due to the need of having a complete cancellation of the reflection, and this happens if the intensities of the two reflected light waves on the upper and lower interfaces are equal, namely:

$$\left(\frac{n_0 - n_{\text{ARC}}}{n_0 + n_{\text{ARC}}}\right)^2 = \left(\frac{n_{\text{ARC}} - n_s}{n_{\text{ARC}} + n_s}\right)^2, \tag{A.16}$$

which leads to the solution $n_{\text{ARC}} = \sqrt{n_0 n_s} = \sqrt{1 \times 1.52} = 1.23$.

According to the discussion above, we see that there is a possibility to approximately eliminate the reflection. However, this possibility is limited as it assumes that the ARC has a constant refractive index and works for just one wavelength. This thing, in turn, does not match the experimentally measured data of the reflection which involve a range of wavelengths. Therefore, we deal in our research with a graded refractive index ARCs, *i.e.*, the refractive index of this inhomogeneous coating depends on the space $x$. Both the cases of the single or even the multiple layer ARCs could be as special cases of this setting. This depends, of course, on how we choose the function that we want to reconstruct.

# Bibliography


[1] Abdullah H and Louis A K *The approximate inverse for solving an inverse scattering problem for acoustic waves in an inhomogeneous medium* Inverse Problems **15** (1999) pp. 12131229.

[2] Alakel Abazid M, Lakhal A and Louis A K *Non-Destructive Testing of Anti-Reflection Coatings for Solar Cells*, Proceedings of the European Workshop on Renewable Energy Systems (EWRES), (2013).

[3] Alakel Abazid M, Lakhal A and Louis A K *A Stable Numerical Algorithm for the Design of Anti-Reflection Coatings for Solar Cells*, submitted (2014).

[4] Ammari H, Kang H, Lee H, Lim M, and Yu S *Enhancement of Near Cloaking for the Full Maxwell Equations*, SIAM Journal on Applied Mathematics, **73**, 2055-2076 (2013).

[5] Ammari H, Kang H, Lee H, and Lim M *Enhancement of near-cloaking using generalized polarization tensors vanishing structures. Part I: The conductivity problem*, Communications in Mathematical Physics, **317**, 253-266,(2013).

[6] Bao G and Wang Y *Optimal design of antireflection coatings with different metrics*, Journal of the Optical Society of America / A, vol. 30, Issue 4, 656-662 (2013).

[7] Belai O.V, Frumin L.L, Podivilov E.V, and Shapiro D.A *Inverse scattering for the one- dimensional Helmholtz equation: fast numerical method.* Optics Letters 33 (2008), 2101-2103.

[8] Born M and Wolf E *Principle of Optics* , Cambridge University Press 7th edn 1999

[9] Bruckner G and Elschner J *A two-step algorithm for the reconstruction of perfectly reflecting periodic profiles*, Inverse Problems **19** p 315-329 (2003)

[10] Chen C J *Physics of Solar Energy* , JOHN WILEY and SONS, INC. 2011

[11] Chen D *Anti-reflection (AR) coatings made by sol-gel process.* Solar Energy Materials and Solar Cells 68,2001, 365-391.

[12] Chen Y, and Rokhlin V, *On the inverse scattering problem for the Helmholtz equation in one dimension.* Inverse Problems **8** 365-391, (1992).

[13] Colton D and Kress R *Inverse Acoustic and Electromagnetic Scattering Theory.* Springer Verlag, 2nd ed. Germany: Berlin, Heidelberg, 1998.

[14] Dautray R and Lions J L *Mathematical Analysis and Numerical Methods for Science and Technology.* Volume 3. Springer Verlag, Germany: Berlin, Heidelberg,1990.

[15] Davis P J and Rabinowitz P *Methods of Numerical Integration.* 2nd ed. Academic Press, INC. New York, 1984.

[16] Dimitriev V I and Chernyavskii A S *Integral Characteristic Method in the Inverse Problem of Optical Coating Design.* Computational Mathematics and Modeling **12**, pp 128-136 (2001).

[17] Dobson D C *Optimal design of periodic antireflective structures for the Helmholtz equation.* Eur.J.Appl.Math.**4**, p 321-339 (1993)

[18] Dudley D G *Mathematical Foundations for Electromagnetic Theory.* IEEE Press, New Jersey: Piscataway, 08855-1331.

[19] Dunn M H, and Hariharan S I *Numerical computations on one-dimensional inverse scattering problems.* NASA Contractor Report 55 (1984), 157-165

[20] Elschner J and Hu G *Global uniqueness in determining polygonal periodic structures with a minimal number of incident plane waves* , Inverse Problems **26** 115002 (2010)

[21] Engl H, Hanke M, and Neubauer A *Regularization of Inverse Problems.* Kluwer, Dordrecht, London, Boston, 2000.

[22] Golub G H and Van Loan F *Matrix Computations.* 2nd ed. Johns Hopkins University Press. Baltimore and London, 1989.

[23] Groh A, Krebs J, and Wagner M *Efficient solution of an inverse problem in cell population dynamics.* Inverse Problems **27** 065009 (2011)

[24] Hahn B and Louis A K *Reconstruction in the three-dimensional parallel scanning geometry with application in synchrotron-based x-ray tomography.* Inverse Problems **28** 045013 (2012)

[25] Hagin F *Some numerical approaches to solving one-dimensional inverse problems.* Journal of Computational Physics 43 (1981), 16-30.

[26] Hanselman D and Littlefield B *Mastering MATLAB 6: a comprehensive tutorial and reference* . Prentice Hall, Upper Saddle River, New Jersey, 07458 (2001).

[27] Hermann G T, Langenberg, H K, and Sabatier P *Basic methods of tomography and inverse problems.* Bristol: Adam Hilger (1987).

[28] Heuser H *Gewöhnliche Differentialgleichungen.* Teubner, Germany: Stuttgart, 3rd ed, 1995.

[29] Hochstadt H *Integral Equations.* Wiley-Interscience Publication, USA: New York, 1989.

[30] Ishimaru A *Electromagnetic Wave Propagation, Radiation, and Scattering.* Englewood Cliffs, N.J. : Prentice Hall, 1991.

[31] Janicki V, Sancho-Parramon J, and Zorc H *Refractive index profile modelling of dielectric inhomogeneous coatings using effective medium theories* 0.5em minus 0.4emThin Solid Films **516**, 3368-3373 (2008).

[32] Kak A.C and Slaney M *Principles of Computerized Tomographic Imaging.* IEEE PRESS, USA: New York, 1988.

[33] Kress R *Linear Integral Equations.* Springer Verlag, 2nd ed. USA: New York Inc. v.82. (1999).

[34] Kohr H and Louis A K *Fast and high-quality reconstruction in electron tomography based on an enhanced linear forward model* . Inverse Problems **27** 045008 (2011)

[35] Kohr H *A linear regularization scheme for inverse problems with unbounded linear operators on Banach spaces.* Inverse Problems **29** 065015 (2013)

[36] Lakhal A and Louis A K *Locating radiating sources for Maxwell's equations using the approximate inverse* Inverse Problems **24** 045020 (18pp) (2008).

[37] Lakhal A *A decoupling-based imaging method for inverse medium scattering for Maxwell's equations.* Inverse Problems **26** 015007 (2010)

[38] Lakhal A *KAIRUAIN-algorithm applied on electromagnetic imaging.* Inverse Problems **29** 095001 (18pp) (2013).

[39] Lakhal A *Resolution of Inverse Scattering Problems for the full three-dimensional Maxwell-Equations in Inhomogeneous Media using the Approximate Inverse.* PhD Thesis, Universität des Saarlandes, Saarbrücken (2006).

[40] Langenberg K J, Brandfass M, Mayer K, Kreutter T, Brüll A, Fellinger P, and Huo D *Principles of Microwave Imaging and Inverse Problems.* EARSel ADVANCES IN REMOTE SENSING, **2**, No. 1-I (1993).

[41] Lesnic D *Determination of the index of refraction of anti-reflection coatings.* Math-in-Industry Case Studies Journal, Volume2,2010, pp. 155-173

[42] Louis A K *Inverse und schlecht gestellte Probleme.* Teubner, Germany: Stuttgart, 1989.

[43] Louis A K *Approximate inverse for linear and some nonlinear problems.* Inverse Problems **12**, pp. 175-190, (1996).

[44] Louis A K *Constructing an approximate inverse for linear and some nonlinear problems in engineering.* Inverse problems in engineering-Theory and Practice, (1998).

[45] Louis A K *A unified approach to regularization methods for linear ill-posed problems.* Inverse Problems **15**, pp. 489-498, (1999).

[46] Louis A K *Combining image reconstruction and image analysis with an application to two-dimensional tomography* SIAM J. Imag. Sci. **vol 1** (p188208) (2008)

[47] Louis A K *Feature Reconstruction in Inverse Problems* Inverse Problems **27** 065010 (21pp) (2011)

[48] Louis A K and Maass P *A mollifier method for linear operator equations of the first kind* Inverse Problems **6** pp. 427440 (1990).

[49] Mahdjoub A, and Zighed L *New designs for graded refractive index antireflection coatings.* Thin Solid Films 478 (2005), 299-304.

[50] Markel V A, O'Sullivan J A, and Schotland J C *Iverse problem in optical diffusion tomography.* IV. Nonlinear inversion formulas. J. Opt. Soc. Am. A, **20**, 903-912 (2003).

[51] Moskow S and Schotland J C *Numerical studies of the inverse Born series for diffuse waves.* Inverse Problems **25**, 095007 (2009).

[52] Müller C *Foundations of the mathematical theory of electromagnetic waves.* Springer-Verlag, Germany: Berlin, 1969.

[53] Natterer F *An error bound for the Born approximation.* Inverse Problems **20**, pp. 447-452, 2004.

[54] Nubile P *Analytical design of antireflection coatings for silicon photovoltaic devices.* Thin Solid Films 342, 257-261, (1999).

[55] Rieder A *Keine Probleme mit inversen Problemen.* Vieweg+Teubner Verlag, Gerrmany: Braunschweig, 2003.

[56] Riplinger M and Spiess M *Asymptotic properties of the approximate inverse estimator for directional distributions.* Advances in Applied Probability Volume 44, Number 4 (2012) 954-976.

[57] Sacks P *An inverse problem in coupled mode theory.* Journal of Mathematical Physics, volume **45**, Number **4**, 1699-1710 (2004).

[58] Schuster T and Schöpfer F *Solving linear operator equations in Banach spaces non-iteratively by the method of approximate inverse* . Inverse Problems **26** 085006 (2010)

[59] Schuster, T *The method of Approximate Inverse: Theory and Applications.* Springer, 2007.

[60] Snieder R *An extension of Backus-Gilbert theory to nonlinear inverse problems.* Inverse Problems **7**, pp. 409-433, (1991).

[61] Snieder R *The role of nonlinearity in inverse problems.* Inverse Problems **14**, pp. 387-404, (1998).

# Affidavit

I hereby swear in lieu of an oath that I have independently prepared this thesis and without using other aids than those stated. The data and concepts taken over from other sources or taken over indirectly are indicated citing the source. The thesis was not submitted so far either in Germany or in another country in the same or a similar form in a procedure for obtaining an academic title.

Saarbrücken, 2014 Mohammad Alakel Abazid.